Department of
Earth Sciences

Groundwater Recharge Model for Gabriola Island

R. Burgess and D.M. Allen

Department of Earth Sciences, Simon Fraser University

Final Report

Submitted to:

Regional District of Nanaimo

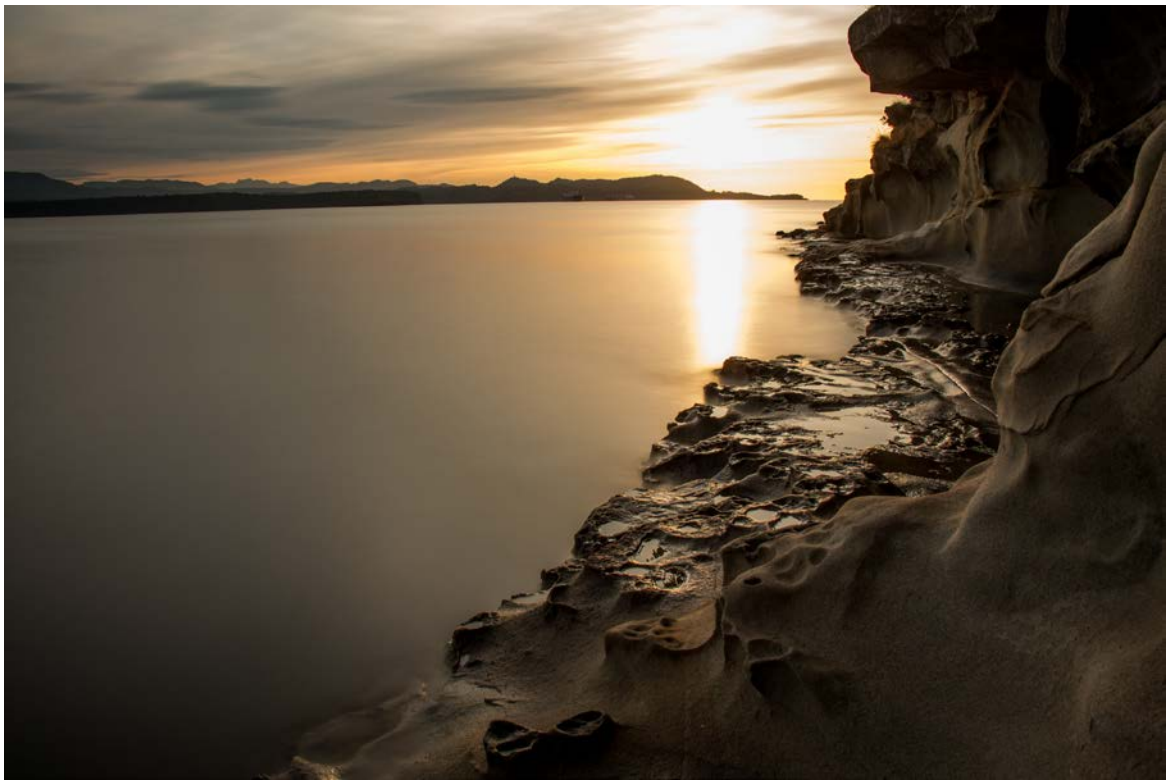

Cover photo: Glenn Jasechko

December 2016

Executive Summary

The overall goal of this research project was to constrain estimates of groundwater recharge on the Gulf Islands. Gabriola Island was used as a case study. Better constrained recharge estimates will enable better estimates of the water balance components, which are needed for water supply and demand studies. This report documents the information collected and interpreted to formulate a conceptual hydrogeological model of Gabriola Island, briefly describes the numerical model setup and calibration, and presents the modeling results.

Overall, there is likely minimal variability in the climate of Gabriola Island such that precipitation, temperature and PET can all be considered spatially uniform. While there is variability in soil types, vegetation is considered to be relatively uniform (treed over 70% of the island). There are few surface water features, and generally only ephemeral streams form during the rainy season. There is variability in the hydraulic properties of the fractured bedrock on Gabriola Island at a local scale, and with depth. However, on a regional scale the fractured bedrock is relatively homogenous and can be represented as a single hydrogeological unit. A decrease in hydraulic conductivity with depth suggests that below a depth of approximately 200 m, groundwater flow is negligible.

A fully integrated land surface – subsurface numerical model was developed for Gabriola Island using state of the art software MIKE SHE. The model was first forced by historical observed climate, and then by projected climate. Actual evapotranspiration, overland flow (runoff), recharge and groundwater seepage were simulated. Overall there is a good match between the averaged simulated and observed WELLS database groundwater levels and the model error is randomly distributed. However, the model slightly overestimates the groundwater levels, with a mean error of -4.4 m. The timing of groundwater level variations is well reproduced by the model. Recharge increases from October to January, where it reaches a pseudo-stable rate, before declining from April through to September. The simulated actual evapotranspiration (AET) had the widest range (35-55% of mean annual precipitation), while recharge displayed the least amount of variability (17 to 26% of mean

annual precipitation). The simulated mean annual recharge to Gabriola Island is 20% of precipitation (or 199 mm/year).

The 2050s and 2080s climate change simulations produce very similar recharge results, only differing slightly during the high recharge periods, with the 2080s being higher. The greatest difference is in the summer months when monthly recharge is projected to decrease by 5-10 mm/month due to a significant increase in evapotranspiration over this time of year. In contrast, the monthly recharge in the winter is projected to increase, but only by less than 5 mm/month due to an increase in precipitation in this season. However, most of the increase in precipitation results in runoff, with a lesser amount occurring as recharge. Overall, the monthly changes in recharge result in an approximate 8% and 7% reduction in annual recharge for the 2050s and 2080s simulations, respectively.

Table of Contents

1.0 Introduction 5

2.0 Conceptual Hydrogeological Model 6

2.1 Geography 6

2.2 Climate 8

2.3 Evapotranspiration 10

2.4 Vegetation and Land Cover 12

2.5 Surface Water 13

2.6 Soils and Geology 14

2.7 Hydraulic Properties 17

2.8 Recharge 20

2.9 Groundwater Flow and the Water Balance 24

2.10 Groundwater Geochemistry 25

2.11 Summary 26

3.0 Numerical Modeling 27

2.9 The Modeling Framework 27

2.10 The Modeling Code 27

2.11 Model Setup 28

2.12 Climate Data 29

2.13 Land Surface Data 29

2.14 Unsaturated Zone (UZ) Data 30

2.15 Saturated Zone (SZ) Data 32

2.16 Boundary and Initial Conditions 33

2.17 Particle Tracking 34

2.18 Climate Change 35

2.19 Calibration Data 38

2.20 Groundwater Abstraction 40

2.21 Model Calibration and Validation 41

Transient Calibration 42

Average Groundwater Level Calibration 44

Model Validation 47

Sensitivity Analysis 47

4.0 Results 48

4.1 Water Balance 48
4.2 Capture Zones 50
4.3 Spatial and Temporal Variations in Recharge and Seepage 51
4.4 Future Recharge 56
4.5 Model Limitations 57
5.0 Conclusions 58
6.0 Acknowledgements 59
7.0 References 60

1.0 Introduction

Previous hydrogeological and water balance studies on the Gulf Islands have attempted to estimate groundwater recharge using a variety of approaches ranging from using rough percentages of precipitation (often estimated at 20% of precipitation), the water table fluctuation (WTF) method (Hodge, 1978, 1995; SRK Consulting, 2013), one dimensional recharge models (Appaih-Adjei, 2006), and two-dimensional groundwater flow models (Liteanu, 2003; Trapp, 2011). Recharge estimated on the basis of a rough percentage of precipitation is based on experience and comparisons to other areas. The WTF approach relies on an estimate of the specific yield (Sy) of the aquifer, and because Sy estimates are difficult to obtain, the recharge results are highly unconstrained. One dimensional vertical percolation (recharge) models assume only vertical flow, such that all infiltrating precipitation enters the groundwater system and does not re-emerge at some location down slope. Consequently, estimates from one-dimensional recharge models tend to yield very high estimates of recharge (upwards of 45% of annual precipitation in areas with high relief (Appiah-Adjei, 2006). While such high estimates are possible for humid regions, the values obtained for the Gulf Islands are inconsistent with other approaches, and thus, are highly uncertain. Typical groundwater flow models assume some value for recharge as input to the model and attempt to reproduce observed groundwater levels. The model calibration process can help to constrain model input values, but the high uncertainty in hydraulic conductivity makes constraining recharge difficult (Trapp, 2011).

To overcome these challenges, three dimensional coupled land surface-subsurface flow models can be used. Such models simulate the water balance at the ground surface, incorporating differences in soil, land cover and topography. They can route water as surface runoff, simulate the interaction between the groundwater and surface water bodies, as well as simulate the groundwater flow system. Foster (2014) used MIKE SHE (Danish Hydrological Institute (DHI)), a fully integrated land surface – subsurface model to model the Cowichan Watershed on Vancouver Island. The overall success of that model at reproducing snowpack in the high elevation areas of the watershed, Cowichan Lake level, streamflow in

the Cowichan River, and groundwater levels in deep and shallow aquifers prompted this study for Gabriola Island. Moreover, Dr. Allen was a technical advisor on the SRK Consulting groundwater study on Gabriola Island (SRK Consulting, 2013). That hydrogeological investigation provided a strong conceptual hydrogeological model of the island as well as detailed datasets that could be used to develop a groundwater recharge model of Gabriola Island.

The overall goal of this research project was to constrain estimates of groundwater recharge on the Gulf Islands using Gabriola Island as a case study. Better constrained recharge estimates will enable better estimates of the water balance components, which are needed for water supply and demand studies. This report documents the information collected and interpreted to formulate a conceptual hydrogeological model of Gabriola Island, briefly describes the numerical model setup and calibration, and presents the modeling results. Additional details concerning the modeling can be found in Burgess (in prep).

2.0 Conceptual Hydrogeological Model

2.1 Geography

Gabriola Island is situated at the northern end of the southern Gulf Islands archipelago, east of Nanaimo on Vancouver Island (Figure 1). It is bordered to the west by Vancouver Island, to the south by other Gulf Islands: Mudge, DeCourcy, and Valdes, and to the east by the Strait of Georgia. Gabriola is about 14 km long and 4.2 km wide, with a land area of 57.73 km^2.

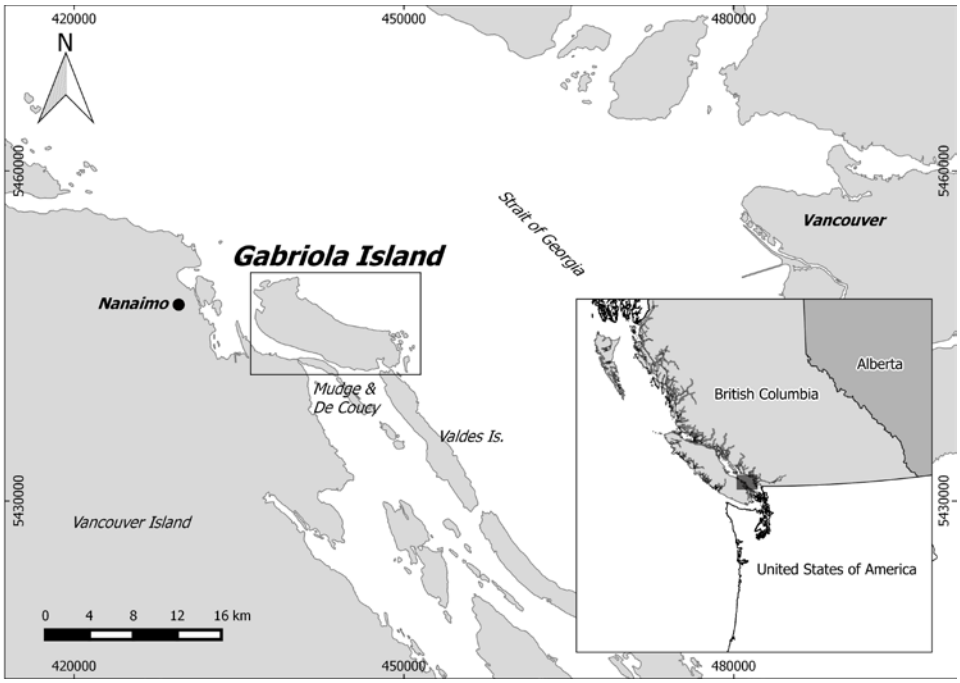

Figure 1. Location of Gabriola Island in western British Columbia (inset map).

The topography of Gabriola Island, shown in Figure 2, is largely controlled by the underlying bedrock. The bedrock consists of alternating sandstone- and mudstone- dominant units. The less competent mudstone units have been preferentially weathered compared to the sandstone units, such that the sandstone forms distinct ridges. Generally the land surface is higher along the southwest of the island, reaching an elevation of 167 metres above sea level (masl). Towards the coast the elevation drops to sea level.

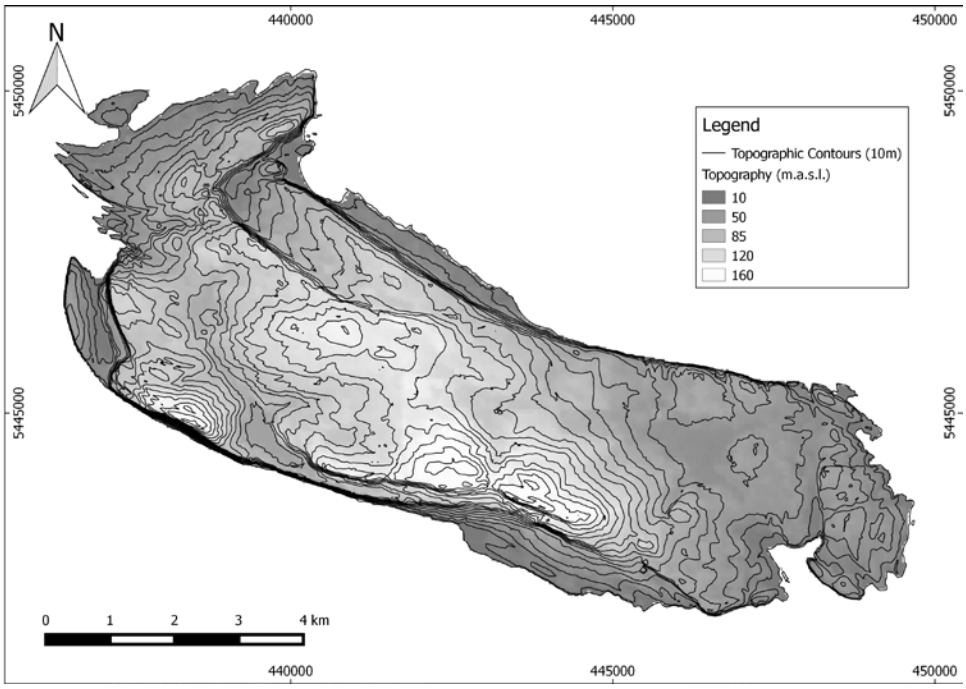

Figure 2. Topography of Gabriola Island

2.2 Climate

Gabriola Island has a mild, temperate climate, with wet winters and dry summers, and lies in the rain-shadow zone of Vancouver Island. There is one active climate station on Gabriola (Climate ID: 1023042), with precipitation and temperature records dating back to March 1967. The mean daily temperature on Gabriola Island ranges from a low of 5.3°C in winter, to a high of 13.9°C in summer (Environment Canada, 2015). The mean annual precipitation (1981-2010) is 958 mm (Environment Canada, 2015). The majority of the precipitation falls as rain, with only a minor amount falling as snow in winter (Figure 3).

There is likely some spatial variation in both the temperature and precipitation across the island. However, due to the relatively low topography, it is unlikely that this spatial variation is significant (SRK Consulting, 2013). Being a temperate climate, there is significant temporal variability in the amount of precipitation. Based on the 1981 to 2010 monthly climate normals data (Environmental Canada, 2015), 25% of the mean annual precipitation falls over the drier summer period (April to September); only <5% falls in the driest months of July and August (Figure 3). Approximately 75% of the mean annual precipitation falls during

the wetter months from October to March. The wettest months are from November to January (~46% of mean annual precipitation).

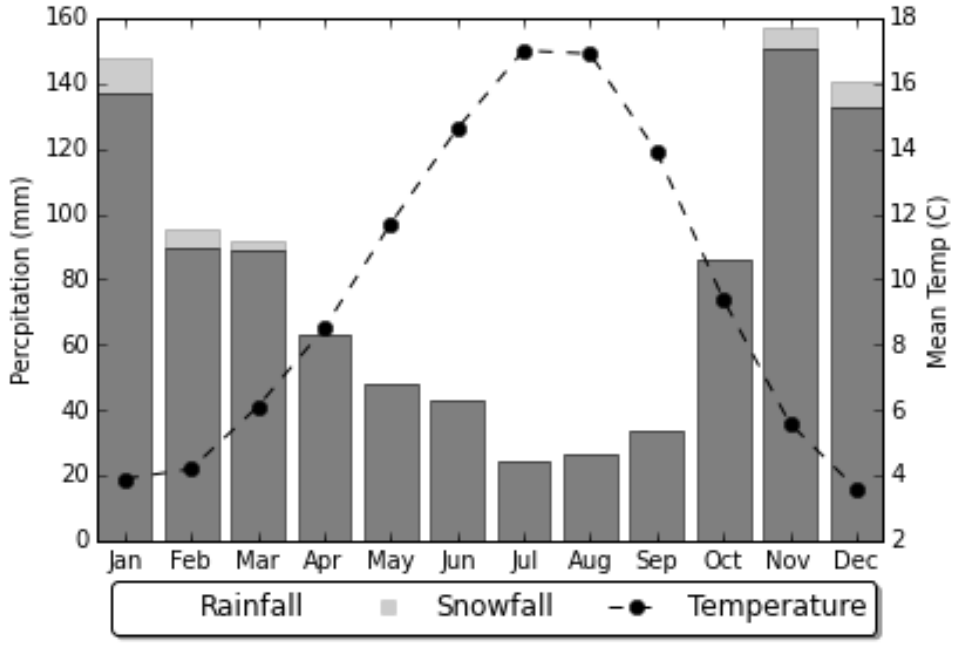

Figure 3. Gabriola Island climate normals (1980 – 2010). Bars represent average monthly precipitation, and the line represents average monthly temperature for Gabriola Island climate station (Climate ID: 1023042).

There is also inter-annual variation in precipitation (Figure 4). Annual precipitation ranges from 800 to 1000 mm in most years. Over the period of record, the mean annual rainfall on Gabriola varied from a low of 405 mm to a high of 1270 mm. Temperature varies less inter-annually; however, there appears to be a slight positive trend in median temperatures (Figure 4).

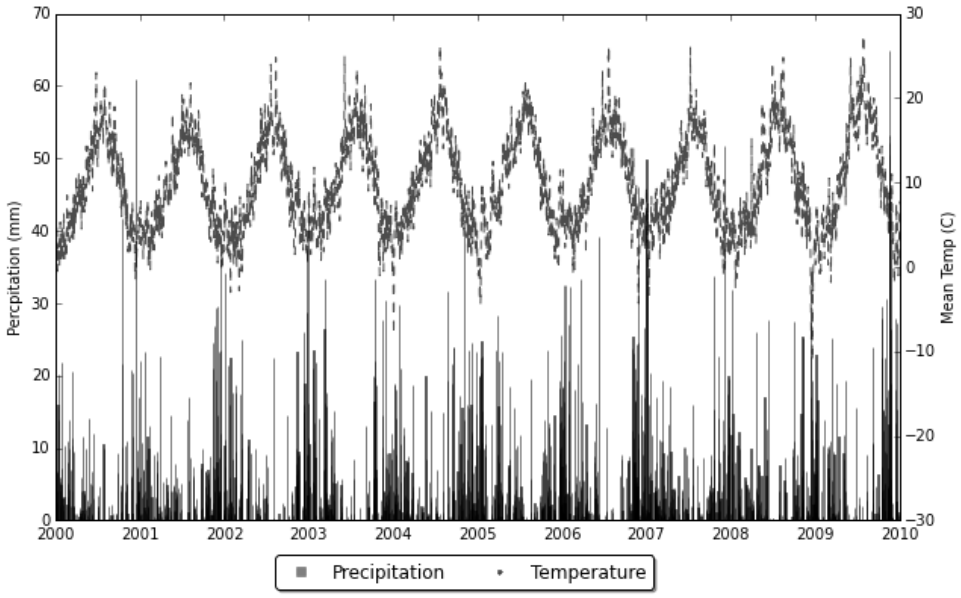

Figure 4. Gabriola Island climate variability. Lower bars represent precipitation, and the upper points represent daily temperature for Gabriola Island climate station (Climate ID: 1023042).

2.3 Evapotranspiration

Evapotranspiration has long been a one of the most difficult components of the hydrological cycle to estimate (Chiew and McMahon, 1991; Zhang et al., 2004). Evapotranspiration may be determined as potential (or reference) evapotranspiration (PET or RET) and actual evapotranspiration (AET). PET is the rate of evapotranspiration from a reference surface, often a hypothetical grass surface with specific characteristics, with an unlimited amount of water, or a measure of the moisture demand from a site (Penman, 1948). It is calculated from only climatic variables, and thus is independent of vegetation. AET is the net result of PET and ability of the reference surface to supply moisture. AET represents the actual amount of water evapotranspired, which is typically less than PET. Quantitative models often use PET to calculate AET.

In this study, PET was approximated following the Penman-Monteith (Monteith, 1981) method using the AWSET software (Cranfield University, 2002). The software calculates PET on a daily basis from temperature, humidity, wind speed, and solar radiation data. Only temperature data were available from the Gabriola climate station; the humidity and wind

speed data were obtained from the nearby Nanaimo Airport climate station (Climate ID: 1025370). The relative humidity and wind speed data were averaged from hourly observations to a daily scale. Solar radiation was approximated using the Solar Radiation Spatial Analyst tool in ArcGIS version 10.0 and interpolation. This tool provides approximations of solar radiation on specified days of a month (the day 15th of every month). Default parameters were used with an overcast sky setting. The daily values were then interpolated using the cubic spline method to provide a continuous daily estimate of solar radiation. The results of the calculated PET are presented in (Figure 5). The results show an seasonal variation in PET. As one would expect, high PET occurs during the summer months, when temperature and solar radiation are highest, and then drops to low values during the winter months. There is only a small amount of inter-annual variation in the calculated PET results.

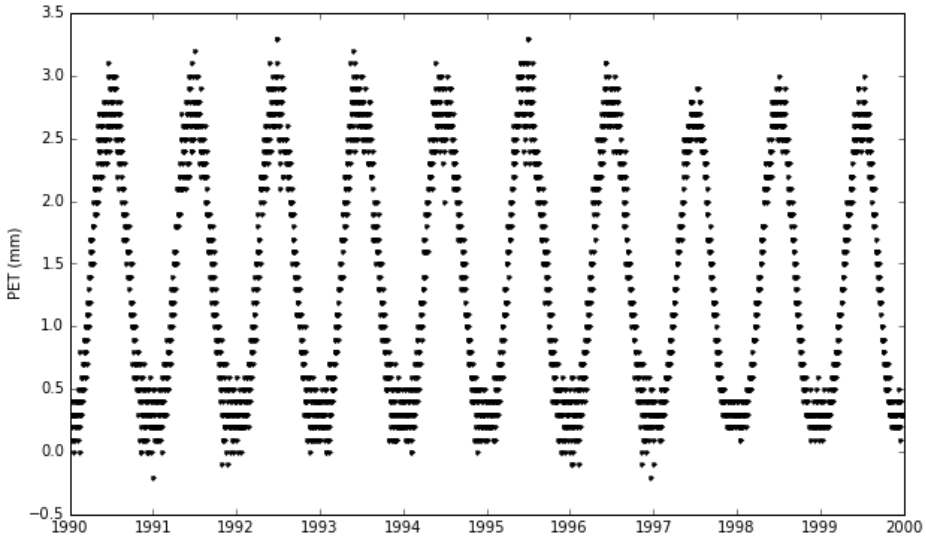

Figure 5. Calculated PET. PET was calculated using the AWSET software (Cranfield University, 2002).

No AET estimates have been made for Gabriola Island specifically; however, previous studies have estimated it for other Gulf Islands, other areas in BC, and for Canada as a whole. Liu et al. (2003) mapped the AET across Canada utilizing a remote sensing approach. Along the 49th parallel (the approximate location of Gabriola Island), the authors estimated AET to be between 250 to 350 mm/yr, or approximately 26-36% of mean annual precipitation on

Gabriola Island. Fernades et al. (2007) used a land surface model in a Canada wide study and estimated an annual AET flux of 385 mm (equating to approximately 40% of mean annual precipitation on Gabriola Island) for the Pacific Coast region. Spittlehouse and Black (1979) estimated the AET from a Douglas fir forest on the southwest coast of BC using temperature and wind speed measurements in an energy balance method. For a period in July 1976, they calculated an average AET rate of approximately 5 mm per day, or over six times the average daily precipitation rate during July (~0.7 mm/day). Appiah-Adjei (2006) and Foster (2014) calculated estimates of AET from numerical models for other Gulf Islands and a watershed on Vancouver Island, respectively, which ranged from 43-50% of mean annual precipitation.

The spatial distribution of AET on Gabriola Island is uncertain. However, during a field visit in June, 2015, the southern side of the island was noticeably drier than northern side, indicating that AET is likely greater on this side of the island. As part of this study, AET on the island was investigated in the field using lysimeters (Burgess, in prep).

2.4 Vegetation and Land Cover

Land cover on the island consists predominantly of forested, agricultural, and residential areas (Figure 6). Based on the spatial data from BC Ministry of Forests, Lands and Natural Resource Operations (FLNRO) (2011), young forest, described as forest less than 140 years old and greater than 6 m in height, makes up approximately 55% of the land cover; urban areas make up approximately 35% of the land cover; with agricultural land, water bodies, recently logged areas, and recreational areas making up the remainder. Although not densely vegetated, trees over 6 m in height are largely ubiquitous throughout urban areas. Thus, the effective area of forest is likely upwards of 70% of the land surface area.

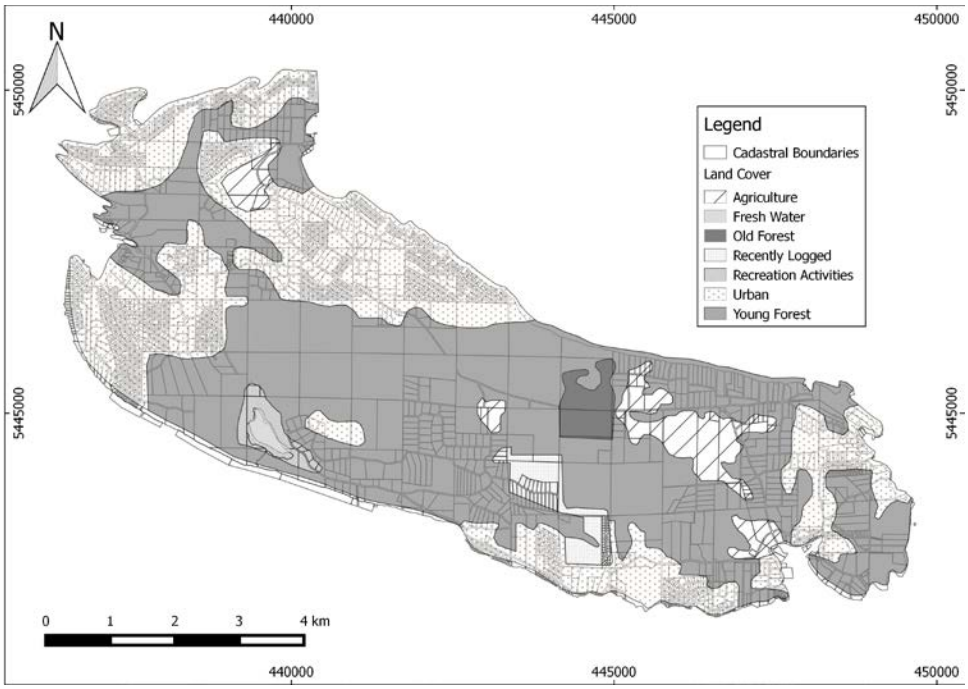

Figure 6. Gabriola Island land cover. Old Forest represents forested areas older than 140 years; Young Forest represents forested areas less than 140 years old; and Recently Logged represents areas logged in the last 20 years. Data from BC FLNRO (2011).

The vegetation of BC has been extensively mapped in the past by the BC Ministry of Forests (BCMoF). Terrestrial ecosystems of BC have been classified according to the biogeoclimatic ecosystem classification (BEC) system (Meidinger and Pojar, 1991). This framework classifies the landscape into map units using a combination of climate and physiographic data, indicating areas that have the ability to support certain vegetation types or ecosystems. Gabriola Island sits within the Coastal Douglas-fir BEC zone. In this zone, the coastal variety of Douglas-fir is the most common (Nuszdorfer et al., 1991), with western red cedar, grand fir, arbutus, Gary oak, and red alder also present, depending on moisture levels and nutrient regimes. The understory of much of the forested areas of Gabriola Island consists of salal.

2.5 Surface Water

There are relatively few surface water bodies on Gabriola Island, with Lake Hoggan being the largest (Figure 7). The majority of the wetlands are seasonal; only a small number are present year round, such as Coats Marsh. Ephemeral creeks only flow for a week or two (SRK

Consulting, 2013). During a field visit in June 2015, the majority of the creeks were dry, with only a few pools at certain locations along steam networks. This observation would indicate that while groundwater does discharge to the creeks through bedrock fractures, this discharge is insufficient to sustain the flow of the creeks during the drier summer months. None of the creeks are currently gauged. Between 1972 and 1978, the level of Hoggan Lake (station number 08HB046) and the outflow of the late at Hoggan Creek (station number 08HB053) were measured by Water Survey of Canada. SRK Consulting (2013) estimated that approximately 60% of annual precipitation occurs as runoff. Welyk and Baldwin (1994) estimated the runoff annual volume from the stream catchments of Gabriola Island at approximately 318 mm per year or 32% of mean annual precipitation.

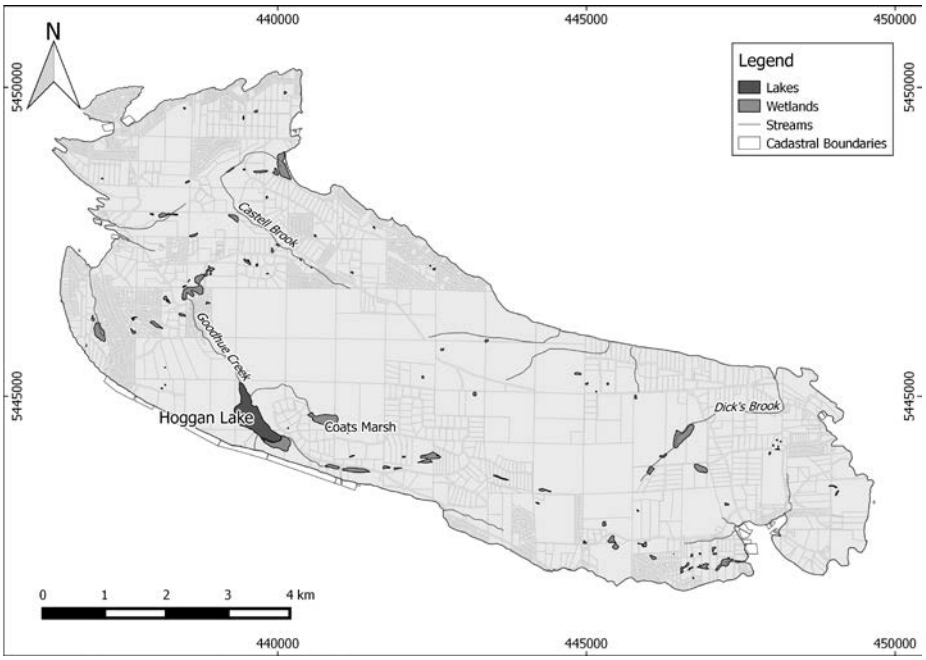

Figure 7. Gabriola Island surface water features.

2.6 Soils and Geology

The soil units of Gabriola Island (and other nearby Islands) were mapped in detail by the BC Ministry of Environment (Kenney et al., 1986). The majority of the soils (>70%) comprise sandy loam/loamy sand overlying bedrock. These soils are generally classed as imperfectly to well drained (Figure 8). Sandstone bedrock is also exposed in some areas.

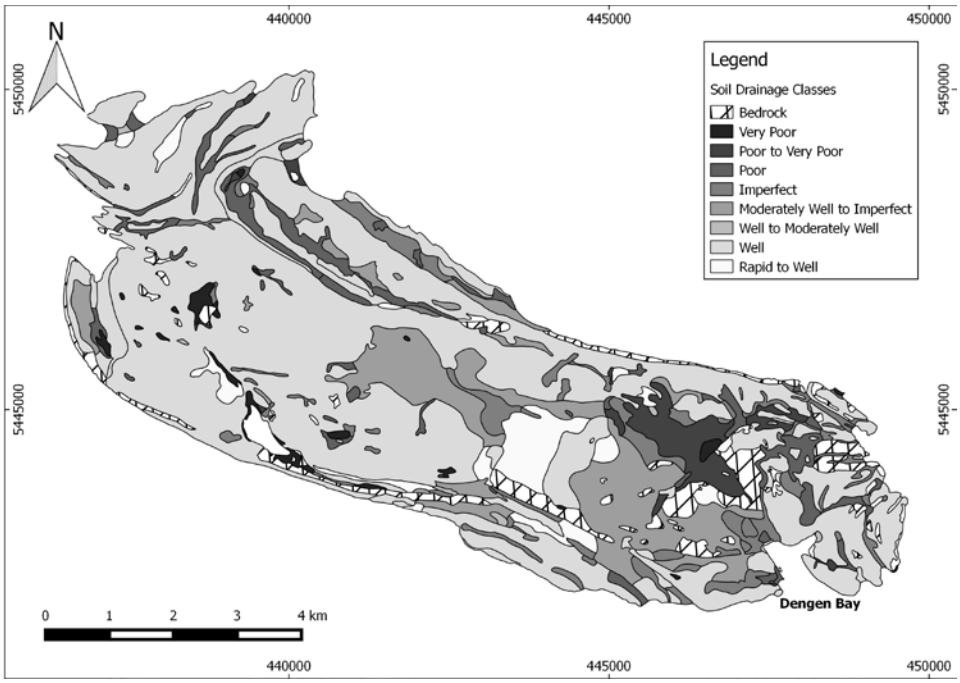

Figure 8. Gabriola Island soil drainability. Data from BC Ministry of Environment (2015a).

Surficial deposits on Gabriola Island are predominantly glaciomarine sediments. Soils are sparse and thin (~2m), and are formed from bedrock weathering and from deposited glacial till and small pockets of glacial outwash (EBA, 2011). The thickest surficial deposits are in the southeast corner of Gabriola Island (up to 25 m of coarse gravel/boulder till deposits) west of Degnen Bay.

The bedrock geology of Gabriola consists of sedimentary formations of the Upper Cretaceous Nanaimo Group (Table 1). These formations are identified as successions of sandstone-conglomerate units interbedded with mudstone and fine-grained sandstone (Mustard, 1994). Four formations of the Nanaimo Group are recognized on Gabriola Island: the Gabriola, Spray, Geoffrey, and Northumberland. The Gabriola and Geoffrey Formations are mainly comprised of sandstone, while mudstone predominantly comprises the Spray and Northumberland Formations (Table 1).

Table 1. Stratigraphy of Gabriola Island. Modified from Mustard (1994).

Formation	Dominant Lithology	Period	Age
Gabriola	Sandstone	Cretaceous	Maastrichtian
Spray	Mudstone		
Geoffrey	Sandstone		
Northumberland	Mudstone		Campanian

The structural characteristics of the Upper Nanaimo Group are the result of two deformation events. First, ancient compression and extension deformation (Mustard, 1994), followed by more recent glacio-isostatic deformation (Clague, 1983). Thus, the bedrock throughout the Gulf Islands has been extensively folded and fractured (Journeay and Morrison, 1999). In addition to fractures, open bedding planes are common on the Gulf Islands; a result of the uplift and/or isostatic rebound after deglaciation (Mackie, 2002). On Gabriola Island, the Gabriola Syncline (a fold) is the dominant structure (England, 1989); this syncline trends northwest to southeast along the length of the island (Figure 9).

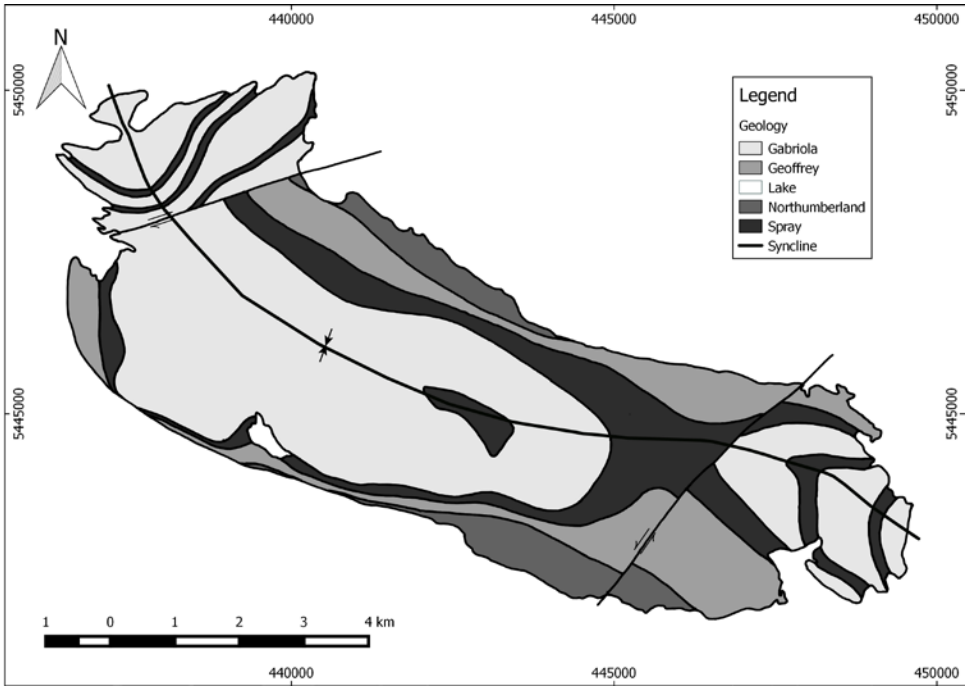

Figure 9. Geology of Gabriola Island. Modified from the B.C. Ministry of Energy and Mines (2005).

2.7 Hydraulic Properties

On Gabriola Island, as on the other Gulf Islands, the fractured bedrock represents the main aquifer material, with the surficial sediments not yielding significant amounts of groundwater (Hodge, 1977). The majority of the groundwater flows through the fractures and joints, bedding planes, and faults; the primary porosity and permeability are low (Dakin et al. 1983; England, 1989; Mackie, 2002). The fractures in the bedrock are considered moderately permeable, and are also easily drained and refilled (low storage capacity).

Several Gulf Islands studies have attempted to characterize the hydraulic properties of the bedrock using various methods, ranging from pumping test analysis (e.g. Larocque, 2014; SRK Consulting, 2013) to developing discrete fracture network models using measurements of fractures mapped throughout the Gulf Islands (e.g. Mackie, 2002; Surrette et al., 2008). Larocque (2014) summarized the hydraulic properties derived from pumping tests conducted throughout the Gulf Islands and found little difference between the average

Transmissivity (T) values for sandstone- ($1.3x10^{-5}$ m^2/s) and mudstone- ($9.5x10^{-6}$ m^2/s) dominant formations (Table 2). K values were calculated by dividing T (calculated from the pumping test analysis results) by the open hole length of the well (base of casing to bottom of hole). There is significant variability in K despite the similar geometric mean values (Table 2). Allen et al. (2002) found the average storativity (S) for the sandstone-dominated formations on the Gulf Islands was $2.7x10^{-4}$ m/s (Table 2). No S values are reported for the mudstone formations. Using open hole length, the average specific storage of the bedrock is $2.0\ x10^{-6}\ m^{-1}$. Figure 10 shows the range of hydraulic conductivity values (K) for the different formations present on Gabriola Island.

Table 2. Summary of hydraulic properties (T values summarized from Larocque, 2014; S from Allen et al 2002)

Rock Type	Transmissivity, T (m^2/s)			Hydraulic Conductivity, K (m/s)	Storativity, S			Specific Storage, Ss
	Geometric Mean	Max Value	Min Value	Geometric Mean	Geometric Mean	Max Value	Min Value	Geometric Mean
Sandstone-dominant	$1.3x10^{-5}$	$5.4x10^{-2}$	$3.4x10^{-7}$	**2.5x10-7**	$2.7x10^{-4}$	$1.8x10^{1}$	$2.8x10^{-9}$	**$2.0\ x10^{-6}$**
Mudstone-dominant	$9.5x10^{-6}$	$6.0x10^{-5}$	$7.6x10^{-7}$	**4.7x10-7**	N/A	N/A	N/A	**$2.0\ x10^{-6}$**

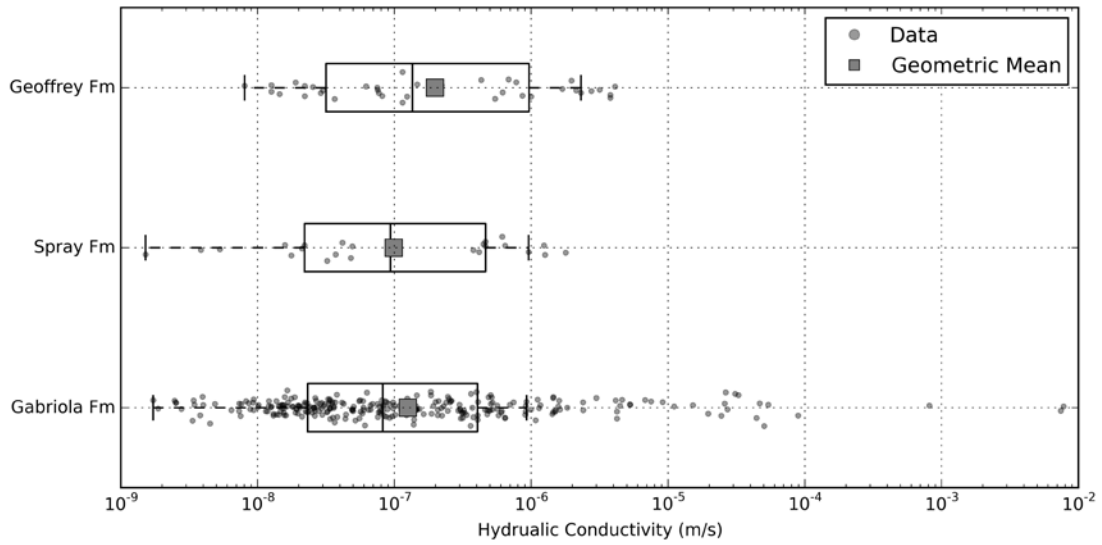

Figure 10. Hydraulic conductivity of Nanaimo Group bedrock. Hydraulic conductivity values originate from pumping test analysis results compiled by Allen et al. (2002). Note: the analysis did not include tests conducted in the Northumberland Formation.

Given the similar hydraulic properties of the Nanaimo Group units across the Gulf Islands, albeit without data from the Northumberland Formation, the formations on Gabriola Island can be conceptualized as a single hydrogeological unit. Moreover, because there are no overlying low permeability layers, the aquifer is likely unconfined. SRK Consulting (2013) suggested that the base of the aquifer coincides with the bottom of the Northumberland Formation, but given that the Northumberland is underlain by the de Courcy formation (sandstone-dominant) there is no geological reason for this to be the case. Rather, the base of the aquifer is more likely related to the depth (or zone) at which the fractures cease to transmit significant flow. Fracture aperture and connectivity often decrease with increasing depth (Snow, 1968, Carlsson et al. 1983). Thus, the hydraulic conductivity of the fractured bedrock aquifer on Gabriola Island likely decreases with depth. Previous studies in fractured bedrock have assumed that flow becomes minimal at a depth of 150-200 m (e.g. Liteanu, 2003; Welch and Allen, 2012; Larocque, 2014; Foster, 2014; Voeckler et al. 2014).

Although the rate of decrease is unknown, simple equations have been derived to estimate the decrease in hydraulic conductivity in fractured rock with depth (e.g. Oda, 1986, Wei et al. 1995, Jiang et al. 2010). Wei et al. (1995) used a hyperbolic equation to describe this decrease in permeability for a fractured rock mass as follows:

$$\frac{k}{k_0} = \left[1 - \frac{z}{A + Bz}\right]^3 \qquad (1)$$

where z is the depth from ground surface to the point of calculation; k and k_0 represent the hydraulic conductivity at surface and permeability at depth, z, respectively; and A and B are two constants. A and B are defined as:

$$A = \frac{z_c}{1 - \left({}^{b_r}/_{b_0}\right)}, \qquad B = \frac{1}{1 - \left({}^{b_r}/_{b_0}\right)} \qquad (2) \text{ \& } (3)$$

where b_r is the residual aperture as depth, b_0 is the effective fracture aperture at depth, and z_c is a reference depth. Wei el al. (1995) estimated values that indicate that b_r is approximately 2.0% of b_0 and z_c is 56.86 m. These values were deemed constant for any fractured rock mass (Wei et al. 1995). By applying the combined average hydraulic conductivity value of 3.6×10^{-7} m/s, from the sandstone- and mudstone- dominated units (Table 3) as k in Eq. (1), the estimated hydraulic conductivity (k_0) of the fractured bedrock on Gabriola Island at 200 m depth below sea level (z) is approximately 3.6×10^{-9} m/s. This is two orders of magnitude lower than that of the upper bedrock. Therefore, a depth of 200 m is considered to reasonably approximate the depth below which flow is insignificant.

2.8 Recharge

Recharge to the Gulf Islands aquifers is dominated by infiltration of precipitation (Allen and Suchy, 2001). Recharge is thought to occur rapidly through the expansive thin, well-drained soils before localized recharge is transmitted through fractures and joints of the fractured bedrock aquifers (SRK Consulting, 2013). Rathay (in prep) observed a groundwater discharge zone along a bedding plane on Gabriola Island

(a seep) respond to a heavy precipitation event in less than 24 hours. The dissipation rate was also rapid. Forty-six hours after the heavy rain event, the seepage area had decreased by approximately 85%. This would indicate that, at least at locally, recharge can occur rapidly though the fractures and joints present in the bedrock.

The dynamics of recharge are recorded in the groundwater level hydrographs. Groundwater levels on Gabriola Island have been recorded by British Columbia's Ministry of Environment since the 1970s. Currently, there are four active monitoring wells that have the depth to groundwater measured. Table 3 provides a summary of the monitoring wells (active and deactivated) and the period of record of each well. The groundwater level on Gabriola Island varies seasonally, with low levels in the dry summer, and high levels in the winter wet season. The hydrographs show that the groundwater level reaches a peak relatively quickly, with no further increase during the continuation of the wet season (Figure 11). This phenomenon is due to the combination of two things: the low storage capacity of the aquifer, and the temperate climate as discussed further below.

The depth to groundwater below the ground surface varies at different locations on Gabriola Island (Figure 11). Although the hydraulic properties of the bedrock units are, on average, very similar, the heterogeneous nature of the fractures may result in the hydraulic properties varying significantly at a local scale. Equally, the location of the well along a groundwater flowpath may influence the depth to groundwater. In discharge zones, the groundwater level is at a shallower depth. Conversely, the groundwater level tends to be deeper in recharge zones. Thus, the depth to groundwater varies. For example, in Figure 11, observation wells OW316 and OW196 have a similar depth to groundwater, whereas the groundwater level at OW197 is approximately 4 m deeper.

Table 3 Observation wells on Gabriola Island

Obs. Well No.	Well Tag No.	Status	Period of Record	
			From	To
196	26709	Active	Oct 1, 1973	Present
197	37811	Active	Aug 1, 1973	Present
385	102208	Active	Jul 9, 2010	Present
316	7895	Active	Sep 2, 1992	Present
194	26710	Deactivated	Aug 1, 1973	2007
317	26350	Deactivated	Sep 2, 1992	2011

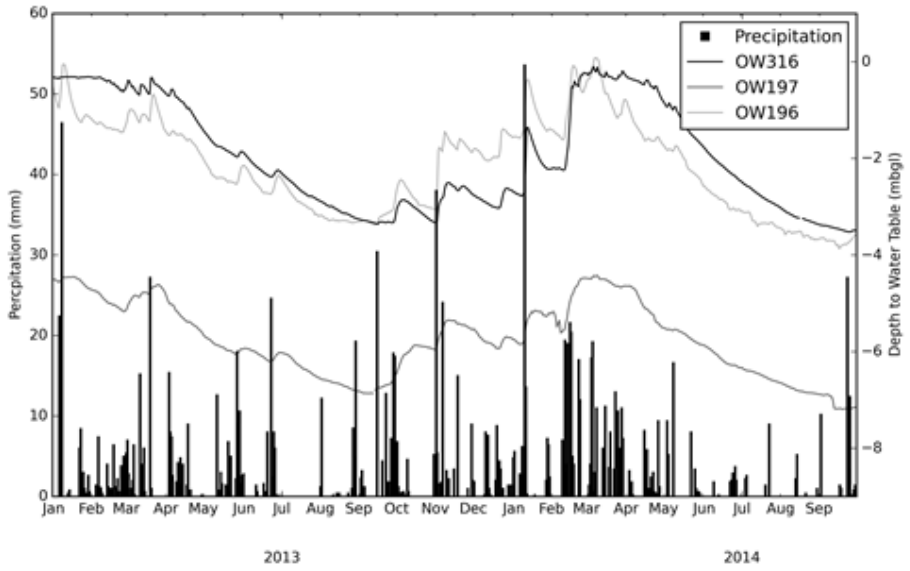

Figure 11. Seasonal groundwater level variation.

Groundwater recharge is seasonally variable. As previously discussed, due to Gabriola Island's temperate climate, 75% of the precipitation occurs in the wet season (October to March). Given the low ET during this period (see Figure 5), it is likely that majority of recharge occurs during this period. The seasonal variability of recharge over an average water year (October 1 to September 30) can be broken down into three distinct phases, which are evident in the groundwater level hydrographs. With the onset of the wet season (early October), the low storage capacity of the fractures results in them being filled, via recharge, relatively quickly, resulting in a rapid water table to rise. Once filled, the recharge

rate slows to equal the rate of discharge (January to April), such that the water table level remains relatively constant. Once the rainfall rate wanes at the end of the wet season, the recharge rate reduces to less than the discharge rate, and the water table lowers over the summer (April to September), until the wet season begins again.

The spatial distribution of recharge is controlled by many factors, such as the type vegetation, amount of AET, changes in topography, soil type, and hydraulic properties of aquifers. At a regional scale, the hydraulic properties of the bedrock units vary little, meaning that this is unlikely to control the spatial distribution of recharge. However, the degree of localized fracturing likely plays an important role in determining groundwater levels and responses at specific locations. While AET is anticipated to vary spatially to some degree, the rapid rate of recharge precludes this from being a significant control on recharge. This leaves the vegetation type, soil type, and changes in topography as the likely controls on recharge. Burgess (in prep) investigates how these three factors control recharge spatially.

Past studies have employed a range of techniques to estimate recharge to the Gulf Islands. The estimates produced from these studies vary widely, from 1% to 72% of mean annual precipitation (Table 4). The techniques employed included: hydrograph analysis (Hodge, 1977, 1995), using the water table fluctuation method (SRK Consulting, 2013), using the USEPA HELP model to simulate the percolation of precipitation though as soil column (Appiah-Adjei, 2006; Denny et al., 2007; Larocque, 2014), and calibration of 3-D numerical groundwater models (Liteanu, 2003; Trapp, 2011). The only study to investigate Gabriola specifically was SRK Consulting (2013). That study utilized the water table fluctuation method to estimate recharge values between 1 and 20% of mean annual precipitation. The authors noted that the likely recharge value lies some in the range of 10-45% of mean annual precipitation based on the range of values reported previously.

Table 4. Recharge estimates of previous studies. nr: no record available.

Study	Study Area	Method	Recharge Estimate (%)	
			Mean	Range
Foweraker (1974)	Mayne	nr	3	nr
Hodge (1977 and 1995)	Salt Spring	Hydrograph	2.6	1 - 4.5
Appiah-Agjei (2006)	Gulf Islands	HELP	45	20 - 60
Denney et al. (2007)	Gulf Islands	HELP	36.5	12.1 - 62.7
Liteanu (2003)	Saturna	Groundwater flow modelling	20	10 - 50
Trapp (2011)	Saturna	HELP	56	5 - 56
SRK Consulting (2013)	Gabriola	WTF method	10	1 - 20
Larocque (2014)	Salt Spring	Groundwater flow modelling	20	3- 45

2.9 Groundwater Flow and the Water Balance

The water table on Gabriola Island mimics topography with high elevation in the center of the island and low elevation towards the coast (Figure 12). As a result, the groundwater generally flows radially from the center of the island towards the coast.

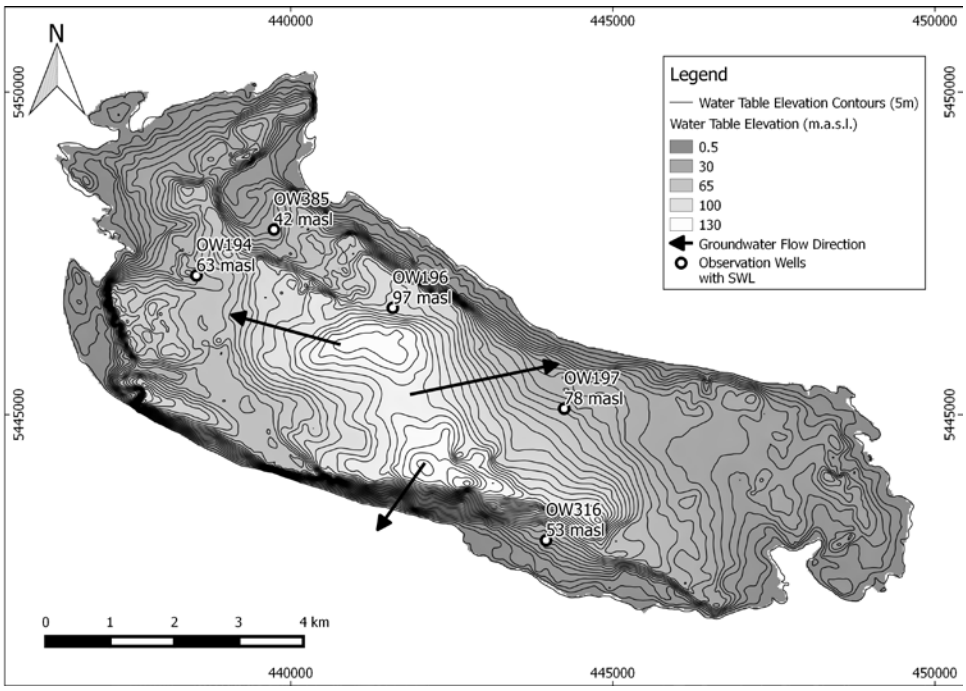

Figure 12. Water table elevation. Interpolation of water table elevation from groundwater levels observed following completion of private wells, modified after SRK Consulting (2013); SWL stands for static water level. The arrows show generalized groundwater flow directions.

No formal water balance has been conducted for Gabriola Island. However, based on the conclusions of previous studies, an initial first-order approximation of the water balance was constructed (Table 5).

Table 5. Estimated water balance. Values are show as a percentage of mean annual precipitation (% of mean annual precipitation).

Water Balance Component	Range (% of mean annual precip)	Initial Estimate (% of mean annual precip)
Evaporation (AET)	32 to 60	45
Runoff	26 to 50	40
Recharge	1 to 62.7	15

2.10 Groundwater Geochemistry

The evolution of the groundwater in the Gulf Islands has been studied on a number of the islands. Based on groundwater samples collected on Saturna Island, Allen and Suchy (2001) proposed that Nanaimo Group groundwaters evolve from being relatively rich in Ca, Mg and HCO_3 near surface, to Na and HCO_3 rich at depth. Sodium enrichment is caused by cation exchange, and is largely ubiquitous given the interbedded nature of mudstones which host clay minerals that act as exchange sites. Salinization is also evident as Na-HCO_3 to Na-Cl, or as Ca-HCO_3 to Na-Cl. This groundwater evolution is also observed in the sedimentary Nanaimo Group rocks on Hornby Island (Allen and Matsuo, 2001), Mayne Island (Allen and Kirste, 2011), and Salt Spring Island (Larocque, 2014).

Earl and Krogh (2004) investigated the groundwater of Gabriola Island, sampling 77 private domestic wells. The authors concluded that the groundwater evolution on Gabriola Island is consistent with processes observed on other Gulf Islands. Figure 13 shows a Piper plot of the groundwater samples. The arrow indicates the direction of geochemical evolution from Ca-HCO_3 water type to Na-HCO_3 water type by cation exchange. Apart from two wells, there is no evidence of salinization in the groundwater sampled in that study.

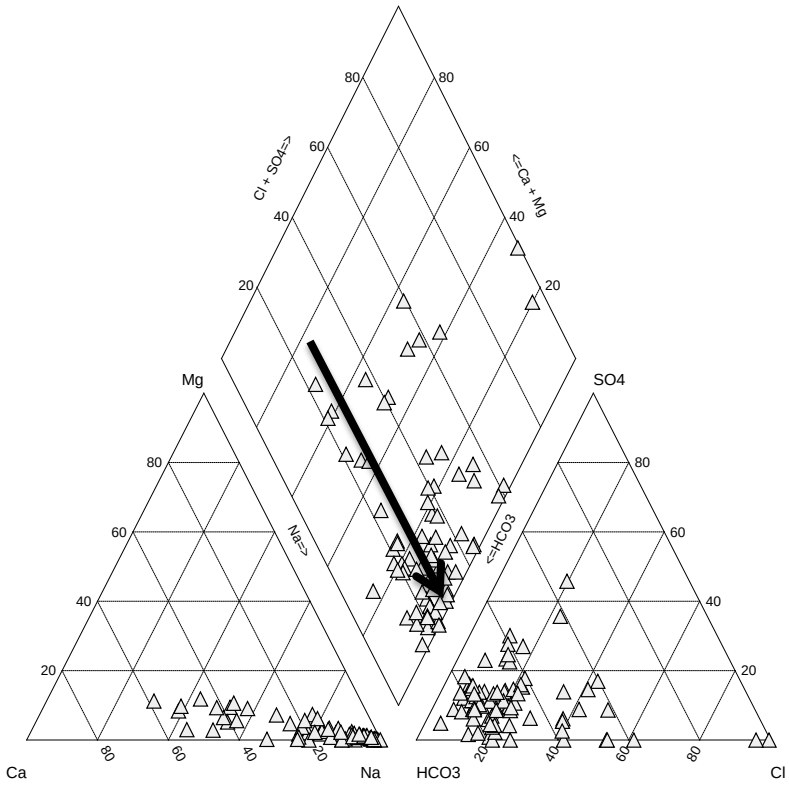

Figure 13. Groundwater geochemistry. Data sourced from Earl and Krogh (2004). All samples were taken from wells with an open borehole construction. The arrow indicates the process of cation exchange, where Ca is exchanged for Na from clay present in the aquifer.

2.11 Summary

Overall, there is assumed to be minimal variability in the climate of Gabriola Island such that precipitation, temperature and PET can all be considered spatially uniform. While there is variability in soil types and land use, the island is generally dominated by one type, thus both can be considered to be relatively uniform regionally. There are few surface water features, and generally only ephemeral streams form during the rainy season. There is variability in the hydraulic properties of the fractured bedrock on Gabriola Island at a local scale, and with depth. However, on a regional scale the fractured bedrock is relatively homogenous and can be represented as a single hydrogeological unit. A decrease in hydraulic conductivity with depth suggests that below a depth of approximately 200 m, groundwater flow is negligible.

3.0 Numerical Modeling

2.9 The Modeling Framework

A coupled groundwater-surface water numerical model was developed to investigate recharge on Gabriola Island. This section documents the development and calibration of the model based on the conceptual model outlined in the previous section. The analysis and discussion of the model results with respect to the recharge dynamics are presented in Section 4.0.

In this modeling study, there were three stages of simulation: a calibration stage, validation stage, and forecast stage. In the calibration stage, the input parameters were adjusted, within a reasonable range, to find the combination of parameters that produces model results that most closely match historic field observations. The calibrated model was then run in the validation stage using climate data from a separate time period to further demonstrate that the model was representing the system dynamics adequately. Finally, the simulation was run into the future, attempting to produce a forecast of the model results for future climate conditions.

2.10 The Modeling Code

MIKE SHE (DHI, 2016) is a state-of-the-art, deterministic, fully-distributed and physically based modeling system that can simulate all of the major components of the land-based hydrological cycle (Jaber and Sukla, 2012). It employs a finite difference approach to solve partial differential equations of overland flow, unsaturated zone flow, and saturated zone flow (DHI, 2007). Evapotranspiration and interception are solved analytically or empirically. The finite difference method uses a network of grid squares to represent the spatial variability of the land surface. The vertical discretization of the model domain is completed through the integration of unsaturated and saturated zone layers. A brief summary of the modules is discussed below (Jaber and Shukla, 2012):

- The interception and evaporation module computes the actual evaporation (AET) from an area using the Kristensen and Jensen model and a user-defined potential evaporation (PET). This model requires vegetation dependent parameters such as leaf area index (LAI) and root characteristics to calculate AET.

- The unsaturated flow in MIKE SHE is only calculated in 1D, vertically. The van Genuchten parameters, along with the saturated hydraulic conductivity, are used to solve the Richards' equation for water flow in the unsaturated zone.

- The overland flow component simulates runoff when infiltration capacity of the soil is exceeded and when groundwater discharges to the surface. The finite difference method utilizes the diffusive wave approximation of the Saint-Venant equation to solve the overland flow water movement. The topographic slope, and the Manning's M coefficient control the direction and rate of runoff, respectively.

- The saturated zone flow component is solved in MIKE SHE using the 3D groundwater flow equation. Boundary conditions such as: fixed head, zero flux, gradient, and specified flux are options which control the flow of groundwater within the model and attempt to mimic real world conditions. Subsurface conditions are modeled as layers and lenses, with representative hydraulic properties assigned.

2.11 Model Setup

The simulation period was from October 1st, 1990 to September 30th, 2015 (with September 30th, 2015 being the most recent date of available climate data for the study region at the time of modeling). The simulation was broken up into two stages: first, a calibration period (15 years) beginning October 1st, 1990; and then a 10 year validation phase to check the performance of the calibrated model from January 1st, 2005 to September 30th, 2015. A daily time step was used.

Since the groundwater and overland flow ultimately discharge to the ocean, the horizontal extent of the domain was specified along the coast of Gabriola Island. A spatially uniform grid size of 150 m provided the best compromise between computation runtimes and model result resolution. The vertical discretization of the unsaturated and saturated zones are described in Burgess (in prep).

Topography plays a key role in the rainfall-recharge-runoff process; thus a 25 m resolution digital elevation model (DEM) was used. This is finest resolution elevation data set available at the time of the study.

2.12 Climate Data

The climate data described in Sections 2.2 and 2.3 were applied to the model, namely precipitation and reference evapotranspiration (RET). Since there is unlikely to be significant variation in precipitation or RET due to the relatively low relief of the island, the climate data were assigned as spatially uniform over the entire model domain. These datasets were set to a temporal frequency to match the simulation time step, i.e. daily.

2.13 Land Surface Data

To calculate actual evapotranspiration, MIKE SHE uses vegetation characteristics and RET. The two principal input components are Leaf Area Index (LAI), and Root Depth. LAI defines the area of leaves per area of ground surface, and the Root Depth is the depth below ground to which roots extend. As previously discussed in Section 2.4, the vegetation on Gabriola Island is primarily Costal Douglas Fir (CDF). Although no studies investigating LAI and rooting depth have focused on Gabriola Island specifically, studies within the same BEC zone have focused on these vegetation characteristics of CDF; providing sufficient reference values. Trofymow et al. (2007) investigated the LAI of CDF near Victoria on Vancouver Island and reported LAI values ranging between 7.1 and 10.3. A similar study on Douglas Fir in Washington State reported an average LAI of 8.6 (Thomas and Winner, 2000). Although LAI varies seasonally (highest in the summer when photosynthesis is most active), for this study, an initial value of 8.5 was determined to be a reasonable annual average. The rooting depth of Coastal Douglas Fir has also not been specifically investigated on Gabriola Island. However, on the eastern coast of Vancouver Island, in the same BEC zone, Black (1979) used rooting depths ranging between 650 and 850 mm to calculate AET. As such, a rooting depth of 750 mm was set. Since the vegetation is relatively uniform across the island, the LAI and rooting depth were set as spatially uniform parameters. Similar to LAI, the rooting depth was also specified to be temporally uniform.

Overland flow is defined as the portion of runoff that occurs as sheet flow. If rainfall exceeds the infiltration capacity of the soil, water will move horizontally across the surface, being

routed by surface topography, at a rate that is calculated in MIKE SHE using the diffusive wave approximation. The resistance to flow overland is controlled by the "roughness" of the land surface, which can be inferred from land use/cover maps. Within MIKE SHE, the Manning's M coefficient (reciprocal of Manning's n), which is equivalent to the Strickler roughness coefficient, controls the amount of friction and the velocity at which water can move horizontally. The value of M is typically in the range of 100 (smooth channels) to 10 (thickly vegetated channels) (DHI, 2007). The United States Department of Agriculture (USDA) (1986) published Manning's n values for vegetated land surfaces ranging between 0.15 and 0.8 for short grass prairie and dense underbrush, respectively. These translate into Manning's M coefficient values of approximately 1 and 7 $m^{1/3}/s$, respectively. In a previous nearby study utilizing MIKE SHE, Foster (2014) used Manning's M coefficient of 2.5 $m^{1/3}/s$ to represent young forest, the dominant land cover on Gabriola Island. Since Gabriola Island is generally covered by relatively dense young forest, a uniformly distributed M of same value was used in this study.

Of the few surface water features present on Gabriola Island, only Lake Hoggan was included in this model. The remaining features, specifically the ephemeral streams, were not included, as they are not present year round (the lake is perennial).

2.14 Unsaturated Zone (UZ) Data

Unsaturated flow within MIKE SHE is calculated only in the vertical direction. In this study, Richards' equation was used to model unsaturated flow. Precipitation that infiltrates the ground surface can either be evapotranspired or flow through the unsaturated zone (UZ) to reach the saturated zone as recharge. The rate and amount of water that flows through the unsaturated zone generally depends on the initial soil saturation, precipitation intensity, and infiltration capacity of a soil. The infiltration capacity of the soil is governed by the saturated hydraulic conductivity and characteristic curve of a soil.

As outlined in the conceptual model (Section 2.6), the soils on Gabriola Island mainly consist of sandy loam with a thickness of approximately 1 m; below this is the fractured bedrock. These two units were specified as spatially uniform, and the UZ column was defined as

vertically uniform in thickness (Figure 14). The sandy loam soil was assigned a depth of 1 m below ground level (mbgl), while the bedrock unit extended to below the base of the Saturated Zone (SZ) (see the next section).

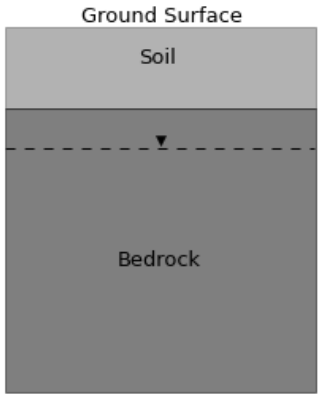

Figure 14. Conceptual UZ column

To solve Richard's equation for unsaturated water flow, the saturated hydraulic conductivity (K_s) and soil characteristic curve of each unit, here soil and bedrock, are required. In this study, these were specified from literature values; the van Genuchten model was used to approximate the soil characteristic curve. Table 6 summarises the unsaturated zone module input parameters.

Table 6. UZ property parameters

Subsurface unit	K_s (m/sec)	Residual Moisture Content (θ_r)	Saturated Moisture Content (θ_s)	α (cm^{-1})	n	Bulk Density (kg/m^3)
Soil[1]	$1.2x10^{-5}$	0.065	0.41	0.075	0.189	1200
Bedrock[2]	$3.0x10^{-7}$	0.05	0.1	0.0036	2.75	2400

[1] Sourced from Leij et al., 1996; [2] Sourced from Voeckler et al., 2004, except for K_s which was approximated from Larocque (2014).

2.15 Saturated Zone (SZ) Data

When modelling the groundwater flow through homogeneous fractured rock, an equivalent porous medium (EPM) approach can be used (Anderson et al., 2015). This approach assumes that groundwater effectively flows through the fractured material as it would in a porous medium (e.g. an alluvial sand aquifer), making no distinction between primary and secondary permeability, and treating the fractures and matrix as a continuum. This simplifying assumption has been used to model the groundwater flow in fractured bedrock on other Gulf Islands (e.g. Liteanu 2003; Trapp, 2011; Larocque 2014). There are limitations to this approach, however. Although the EPM approach may simulate the behaviour of a regional flow system, heterogeneities of fractured rock at a small scale may result in the approach being unable to represent local groundwater flow. This may result in local variations in hydraulic heads, for example, due to the presence or absence of localized fractures. However, for the purposes of this regional model, an EPM approach is a reasonable assumption.

The Saturated Zone (SZ) was represented as a single geological layer, represented by uniform hydraulic properties (Table 7; more detailed discussion is provided in Burgess, in prep). This is reasoned on the assumption that the hydraulic properties of the Nanaimo Group bedrock are relatively homogenous at a regional scale (Section 2.7). In fractured bedrock, the depth at which groundwater flow becomes negligible is around 150 to 200 mbgl (Gleeson et al., 2011; Welch and Allen 2014). Gabriola has a topographical high point of ~160 masl, thus the bottom of the model domain was set to a uniform value of -50 masl. This resulted in a maximum model domain thickness of 210 m and a minimum thickness (near the coast) of 50 m. The thinner model domain near the coast is realistic because here freshwater normally discharges to the ocean in a narrow zone above the freshwater-saltwater interface.

The SZ was discretized as a single computational layer. Therefore, groundwater flow in the SZ is assumed to be generally horizontal from areas of high hydraulic head to low hydraulic head (i.e. toward the coast).

Table 7. Initial estimates of the hydraulic properties assigned to the model

Parameter	Initial Estimate	Range
Hydraulic Conductivity (m/s)	3.0×10^{-7}	5.0×10^{-8} to 5.0×10^{-6}
Specific Yield (-)	0.026[1]	0.01 to 0.1
Specific Storage (m^{-1})	2.0×10^{-6}	$2.0 \times 10^{-8}$to 1.4×10^{-5}
Porosity (%)	8	1 to 10

[1]In MIKE SHE this value is automatically calculated from the UZ parameters used.

2.16 Boundary and Initial Conditions

In the model, the precipitation that falls onto the model domain is routed out of the model via three potential pathways: evaporation, overland flow reaching the ocean, and groundwater discharge to the ocean.

Two specified head boundary conditions were used in the SZ module of this model. To simulate the discharge of groundwater to the ocean, a specified head boundary condition was set around the edge of the model domain (coast of island). Although there are daily tidal fluctuations in sea level, they are not anticipated to have a significant influence at a regional scale. Thus, a temporally uniform value of 0 masl was set to this outer boundary condition. It is important to note that this coast boundary is actually a salt boundary. MIKE SHE cannot simulate density-dependent flow and solute transport; therefore, the specified head cells are placed to allow for a seepage face to develop at the coastline to allow the freshwater to discharge. The setup of this boundary condition implies that the seepage face of groundwater discharge to the ocean is approximately 50 m thick, since the base of the model is specified at 50 mbgl at the coast. The depth of the SZ, and thus seepage face thickness, was tested in the sensitivity analysis (see Burgess, in prep).

A single internal boundary condition was used to represent Hoggan Lake, the only lake of significant size present on the island. A value of 58 m.a.s.l. was extracted from the DEM of the island representing the average lake level. The distribution of the specified head cells is shown in Figure 15.

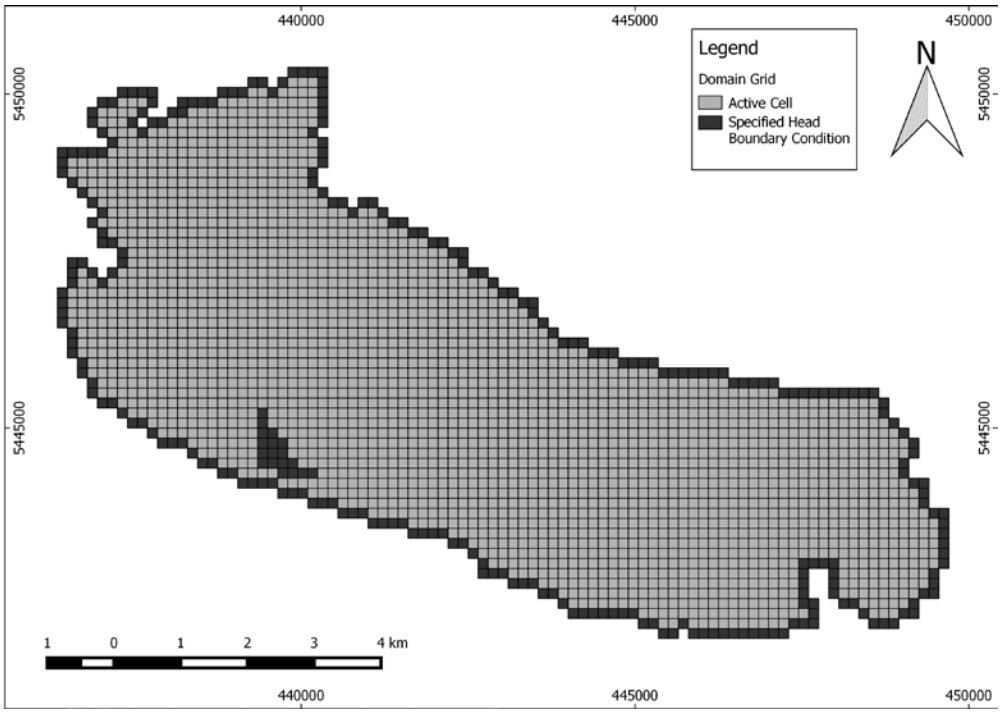

Figure 15. Location of specific head boundary conditions.

An initial head distribution is required to run MIKE SHE. The model spins up from this initial head distribution and gradually converges to a dynamic solution whereby the water level changes temporally, but reflects a stable overall head range. The initial head distribution was specified from a water table interpolated in a previous study shown previously in Figure 12 (SRK Consulting, 2013).

2.17 Particle Tracking

Particle tracking was utilized in MIKE SHE to compare simulated groundwater travel time to qualitative apparent groundwater age estimates from the tritium analysis of sampled groundwaters (see Burgess, in prep). All the groundwater samples tested contained measurable amounts of tritium; therefore, it is inferred that the mean groundwater residence time of each water sample is less than 50 years (see Burgess, in prep).

In MIKE SHE, particle tracking is achieved by releasing a defined number particles into every cell in the SZ module, and then simulating the advective transport these particles. In this study, five particles were released in each cell. While all the particle travel paths are

simulated, only those particles that reach a sink (e.g. constant head boundary condition or pumping well) are registered. Since the samples for tritium analysis were collected from private domestic wells, with no pump usage available, very low flow pumping wells were specified at their location in the model; this enables particles entering the well cell to be registered while having a negligible effect on the water balance. A constant rate of 0.001 m^3/s was set as the pumping rate at each of the four domestic wells. Since the SZ module of the model has only one layer, the depths of the wells were arbitrarily set to 30 mbgl.

Particle tracking simulation was run for a 50 year period. The originating locations of the registered particles was used to further elucidate groundwater flow dynamics.

2.18 Climate Change

Climate change has the potential to affect groundwater resources globally (Green et al., 2011), principally though changes in the climatic patterns of temperature and precipitation. Based on global climate model (GCM) simulations, the future atmospheric temperature, and the amount and intensity of precipitation are predicted to be altered. As discussed previously, temperature and precipitation, in part, directly control the amount of recharge an aquifer receives. An increase in temperature, for example, could potentially increase evapotranspiration (if there is water available) and reduce the amount of recharge to groundwater from precipitation. Consequently, such changes to climate may have significant impacts on the sustainability of groundwater resources in the future.

The GCMs take into consideration socioeconomic scenarios to make projections on how future greenhouse gas (GHG) emissions may change the global climate (Carter et al., 2001). Each model is run for a number of future climate emissions scenarios that include conservative through to optimistic GHG emissions. The GCMs forecast the future climate shifts for specific decades in the future, specifically: the 2020s, 2050s, and 2080s. The global climate change models are produced at a coarse regional scale and are often downscaled using various methods, such as TreeGen (Cannon, 2008). Previous studies (Appaih-Adjei, 2006; Larocque, 2014, Foster, 2014) used the projected change in climate (shifts) to assess

how recharge on the Gulf Islands and Vancouver Island may vary in the future. A similar approach has been employed in this study.

Recharge to Gabriola Island under future climate change conditions was assessed by applying the climate shifts (from GCM outputs) to the climate data input, specifically RET and precipitation. The future climate change predictions were limited to 2050s and 2080s since the 2020s are less than five years away. The GCM data were accessed utilizing the BC Regional Analysis Tool (Pacific Climate Impacts Consortium (PCIC), 2016). For this study, the 'SRES AR4 -!PCIC TreeGen ensemble' was used. The ensemble consists of four downscaled CMIP3 GCMs: the CCCMA_CGCM3, CSIRO_MK30, GFDL_CM20, and MPI_ECHAM5. Various model runs are available for each GCM, and for different emissions scenarios, A1B, A2, and B1, which represent different degrees of forecasted climate change. The A2 scenario was utilized in this study since it represents the most serve impact on climate conditions. It is noted that current trends in observed climate are consistent with the A2 scenario.

The climate shift data extracted from the GCMs focused on the climate properties required for estimation of RET and precipitation (inputs needed in MIKE SHE), namely: changes in mean, max and min temperature, incident solar radiation, relative humidity, and precipitation for the 2050s (2040 to 2069) and 2080s (2070 to 2099). The data were extracted from a clipped region around Gabriola Island. The shifts were applied to a daily historical climate data (2005 to 2015) to form climate datasets representative of the future periods. The GCM data are reported as monthly changes, thus to apply the shifts at a daily frequency the average monthly result of the A2 scenario from differing models (and their runs) were interpolated. This was done by assuming the GCMs results represent the middle of the month (15^{th} day of every month) and linearly interpolating to a daily scale. The type of shift differed between climate properties. Temperature and solar radiation shifts are as absolute changes, while precipitation and relative humidity shifts are as percent changes. The shifted temperature, solar radiation, and relative humidity were used, in the same way as the historical data, to estimate future RET using AWSET (see Section 2.3). Shifts in wind speed are not included in the GCMs results, and therefore, the historical data were used to

estimate RET; this assumes that average daily wind speed will not change significantly in the future.

The average monthly results of the shifts to RET and precipitation for the 2050s and 2080s are presented Table 8.

Table 8. Changes to RET and precipitation under forecast future climate conditions.

	RET (% change)		Precipitation (% change)	
	2050s	**2080s**	**2050s**	**2080s**
January	5	8	10	11
February	7	10	9	13
March	5	8	9	11
April	3	5	16	21
May	4	6	12	19
June	6	9	2	6
July	11	16	-9	-13
August	13	18	-11	-10
September	9	13	8	10
October	5	8	15	17
November	4	7	12	15
December	5	8	7	11

The biggest shifts in precipitation will be realised in the spring, summer and fall. In the spring and fall, precipitation is projected to increase by approximately 10-15% and 10-20% for the 2050s and 2080s, respectively. Conversely, the summer months will see a decrease in precipitation by approximately -5 to -10% for both the 2050s and 2080s. Precipitation in the winter months is projected to increase by a fairly consistent amount, approximately 10% in both periods. The calculated shifted RET indicates that the greatest changes will occur during the summer months, with a 10-12% and 14-18% increase in RET for the 2050s and 2080s, respectively. Lesser changes in RET are projected over the rest of the year, 2-6% and 6-10% increase for the 2050s and 2080s, respectively. Overall, the changes are greatest for both precipitation and RET in the 2080s. These shifts would seemingly accentuate the seasonality of a temperate climate.

Two MIKE SHE simulations (one representing the 2050s and one the 2080s) were run using the shifted precipitation and RET input datasets. The calibrated model groundwater level solution on September 1st 2005 (last time step of simulation) was used as the starting head condition, also known as a hot start. The results of these future projections are discussed in Section 4.0.

2.19 Calibration Data

When modelling groundwater flow it is desirable to have stream flow and groundwater level observation data to constrain the calibration of the model. However, on Gabriola Island none of the streams are gauged. Thus, only groundwater level elevation observation data were available for this study; two datasets were used. First, six provincial observation wells with long term records were available to match the transient response of the model. Although heterogeneities in the hydraulic properties of the fractured bedrock at the local scale may preclude this dataset from being effective for calibration of this regional model, the observation time series is vital for insuring that the timing of the seasonal fluctuations in groundwater level are representative of the physical world. The locations of these observation wells are shown in Figure 16. As discussed previously (Table 3), only three of the six observation wells have measurement records that span both the calibration and validation periods (OW196, OW197, OW316). OW194 and OW317 were only used in the calibration period since they were deactivated in 2007 and 2006, respectively, whereas OW385 was only used in the validation since the period of record of this well only started in 2010.

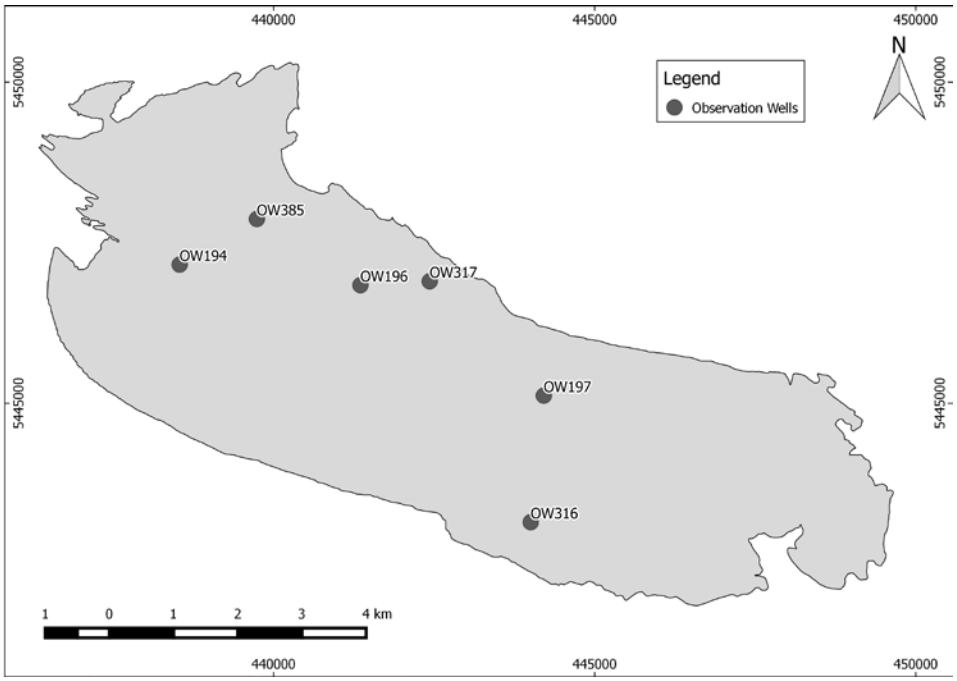

Figure 16. Location of provincial observation wells.

Second, available drilling records provide measurements of the groundwater elevation immediately following the completion well drilling. These data are reported as static groundwater levels in the BC WELLS Database (BC Ministry of Environment, 2015b). These 'average' groundwater levels can be compared to the average simulated transient groundwater level at the same point. The high number (2092 wells) and spatial distribution (Figure 17) of measurements help overcome the limitation of solely using the observation well time series as observation data, providing spatially distributed average groundwater level measurements. However, some caveats in using this second dataset exist, resulting in observation data that are somewhat biased. Firstly, immediately after drilling and completion of water wells the groundwater level will typically be lower than normal because the water level in the well has not fully recovered from drilling. Thus, these measurements can be expected to be lower than under natural conditions. Secondly, the private wells on the Gulf Islands are generally drilled in the summer. Since there is a pronounced seasonal variation in the groundwater levels on Gabriola Island, the measurements can be expected to be lower than the annual average groundwater level. Despite the bias of lower

groundwater levels from the WELLS database, previous studies have used these data to calibrate numerical models (e.g. Larocque, 2014; Foster, 2014).

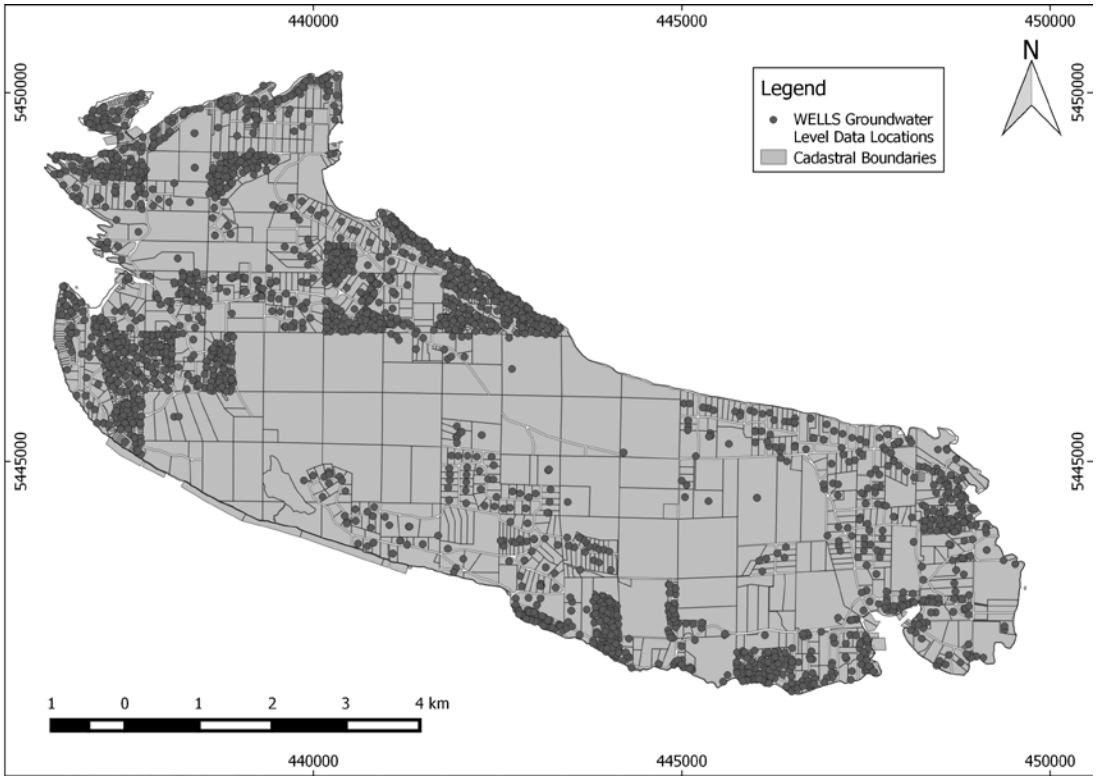

Figure 17. Location of water wells from the WELLS database used for model calibration.

2.20 Groundwater Abstraction

Groundwater abstraction on Gabriola Island mainly occurs through domestic and non-domestic (commercial and agricultural) wells. This abstraction was implemented in the model by including pumping wells in the SZ module of MIKE SHE. Data pertaining to the actual number of active wells and abstraction on Gabriola Island are scarce (SRK Consulting, 2013); thus, and a number approximations were made regarding the location and abstraction rates. Firstly, domestic and non-domestic groundwater wells were not distinguished in the model – both were assigned the same abstraction rate. Second, the pumping wells were represented spatially based on locations in the BC WELLS Database (Figure 17). Third, two constant pumping regimes were assigned; a lower abstraction rate during the wetter times of the year (October to March), and a higher rate during the drier

months (April to September). Due to the aforementioned scarcity of abstraction data, the island wide water demand estimated by SRK Consulting (2013) was used instead of actual abstraction data. For the two pumping regimes, this translated into pumping rates of 0.50 and 1.62 m^3/day for the October to March and April to September periods of each year, respectively. These approximations assume that all the wells are in use every day, and that every well being used is in the database. In reality, neither of these assumptions hold true; however, they are deemed appropriate given the lack of data available. This pumping regime was also applied to future scenarios.

2.21 Model Calibration and Validation

The calibration of the model solely utilised the manual trial and error approach, as MIKE SHE does not have parameter estimation capabilities. The approach focused on varying the hydraulic conductivity of the bedrock within the range reported in Table 7 in an attempt to match simulated groundwater levels with observed groundwater levels. The specific storage of the fractured bedrock and saturated hydraulic conductivity of the soil were also varied initially; however, the model proved to not be sensitive to these input parameters. The van Genuchten parameters of the fractured bedrock were also altered in an attempt to force an increase in the specific yield in the SZ. However, these changes made the model numerically unstable, and were thus abandoned.

The model was calibrated to two different types of groundwater level datasets: (1) the transient observed groundwater levels at observations wells, and (2) the static water levels reported in the WELLS database. Error statistics were used to measure the degree of model fit during the calibration process. These were: mean error (ME), mean absolute error (MAE), root mean squared error (RMSE), Pearson coefficient (P_{cor}), and Nash-Sutcliffe coefficient (N-S) (see Burgess, in progress for a definition of these common error statistics). The ME, MAE, RMSE and P_{cor} error statistics were primarily used to assess the model calibration to the WELLS database observations. The NS was used to assess the dynamics of the simulated groundwater level in the transient calibration stage.

Transient Calibration

The transient phase of calibration aimed to calibrate the timing of the seasonal response of the model. The transient simulated groundwater levels were calibrated against five observation wells on Gabriola Island. The initial value for hydraulic conductivity (see Table 7) was adjusted during calibration. The final hydraulic parameters used are reported in Table 9.

Table 9. Final calibrated hydraulic parameter values.

Parameter	Calibrated Value
Hydraulic Conductivity (m/s)	4×10^{-7}
Specific Yield (-)	0.0018
Specific Storage (1/m)	2.4×10^{-5}
Porosity (%)	8

Figure 18 and Table 10, respectively, show the groundwater water level results and error statistics for the five observation wells. In order to exclude results from the model spin-up period, the error statistics were calculated from October 1st 1992 until the end of the calibration period (September 30th 2005).

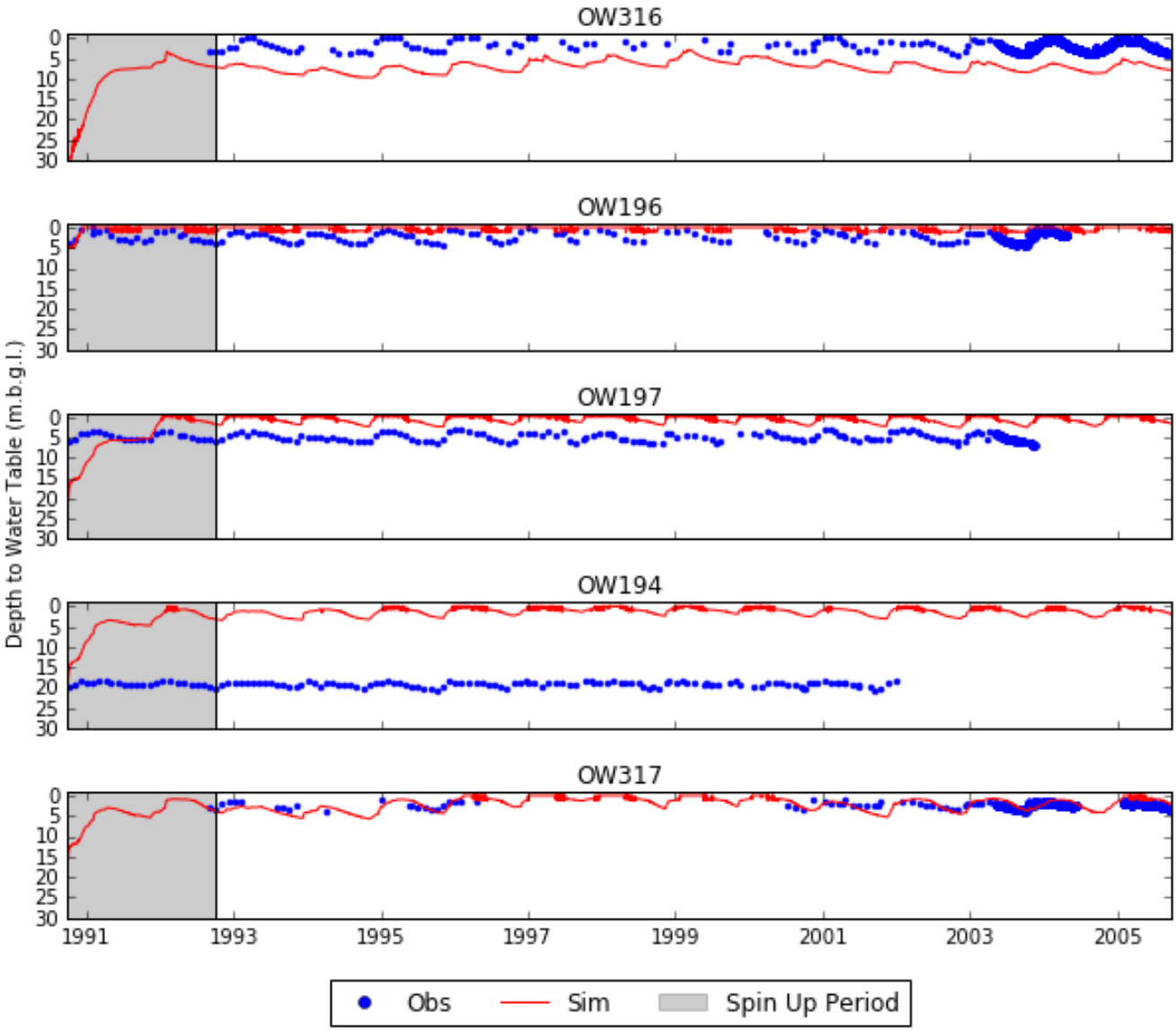

Figure 18 Simulated to observed fit of transient groundwater levels.

Table 10 Calibration observation well error statistics.

Error Statistic	OW316	OW196	OW197	OW194	OW317
ME (m)	3.8	-1.4	-4.4	-18.1	-1.3
RMSE (m)	3.8	1.5	4.4	18.2	1.5
P_{cor}	0.84	0.84	0.59	0.55	0.22
N-S	-9.7	-1.5	-27.8	-985.5	-9.37

The degree fit of the simulated groundwater levels to observed groundwater levels varies between the observation wells. The timing of the groundwater level rise and fall during the year is well represented in the model; this is most apparent in OW316. However, the average simulated groundwater level is consistently less than the observed values at all observation points except OW316 (a negative mean error indicates an over prediction of groundwater levels).

Average Groundwater Level Calibration

This phase of calibration aimed at calibrating the model spatially. The groundwater levels from the approximate end of the spin-up period (October 1st 1992) to the end of the calibration period (September 30th 2005) were averaged to produce a groundwater level dataset which was compared against the groundwater levels from the WELLS database. The results of the calibration are displayed in Figure 19, and the error statistics are reported in Table 11.

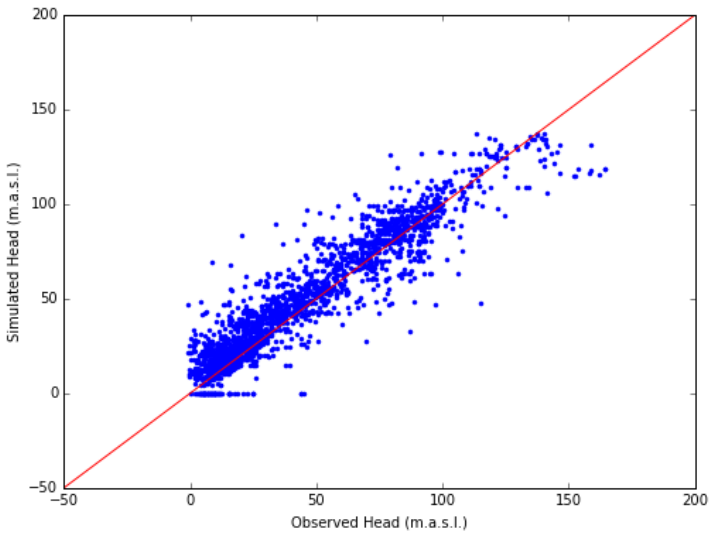

Figure 19. Simulated to observed fit of groundwater levels.

Table 11. Calibration WELLS database error statistics.

Error Statistic	Value
ME (m)	-4.4
MAE (m)	9.0
RMSE (m)	12.5
P_{cor}	0.94

Overall there is a good match between the averaged simulated and observed WELLS database groundwater levels. In Figure 19, the majority of the simulated values plot near the 1:1, and the P_{cor} value of 0.94 in Table 11, represents a reasonable fit to the observed data. The ME value of -4.4 m indicates that overall the simulated groundwater level results are higher than the observed values. However, since the majority of the observation data in the WELLS database are likely less than the yearly average groundwater level, this level of over prediction is acceptable.

A sufficiently calibrated model should also be unbiased, with the residual error randomly distributed both statistically and spatially. The statistical distribution of the residuals is displayed in Figure 20. The residual error is the difference between the observed groundwater level value and the simulated value. Figure 20 clearly shows an approximate Gaussian distribution, which indicates that the residual error is randomly distributed across the model, although the mean of the distribution indicates that the model is over-predicting the groundwater levels as indicated above. The spatial distribution of the residual error is also randomly distributed (Figure 21). In other words, there are no areas in the model domain that are biased towards over or under prediction of groundwater levels.

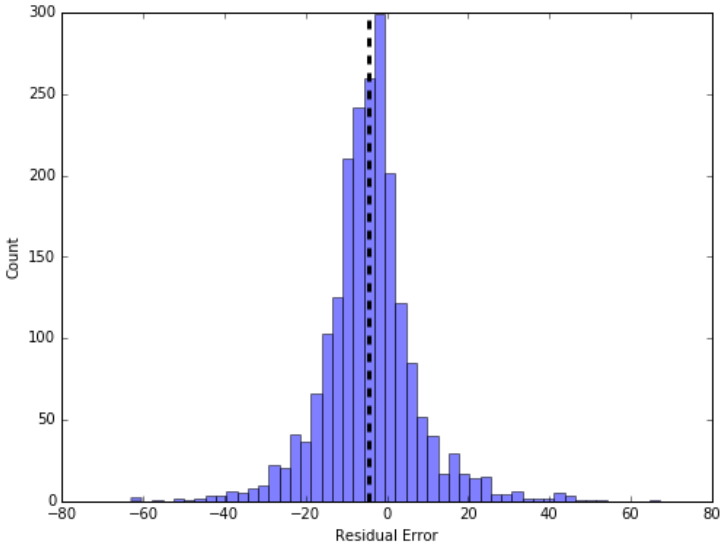

Figure 20 Statistical distribution of error. The mean residual error is represented by the dashed vertical line. The mean of the distribution suggests that the model is over-predicting the groundwater level.

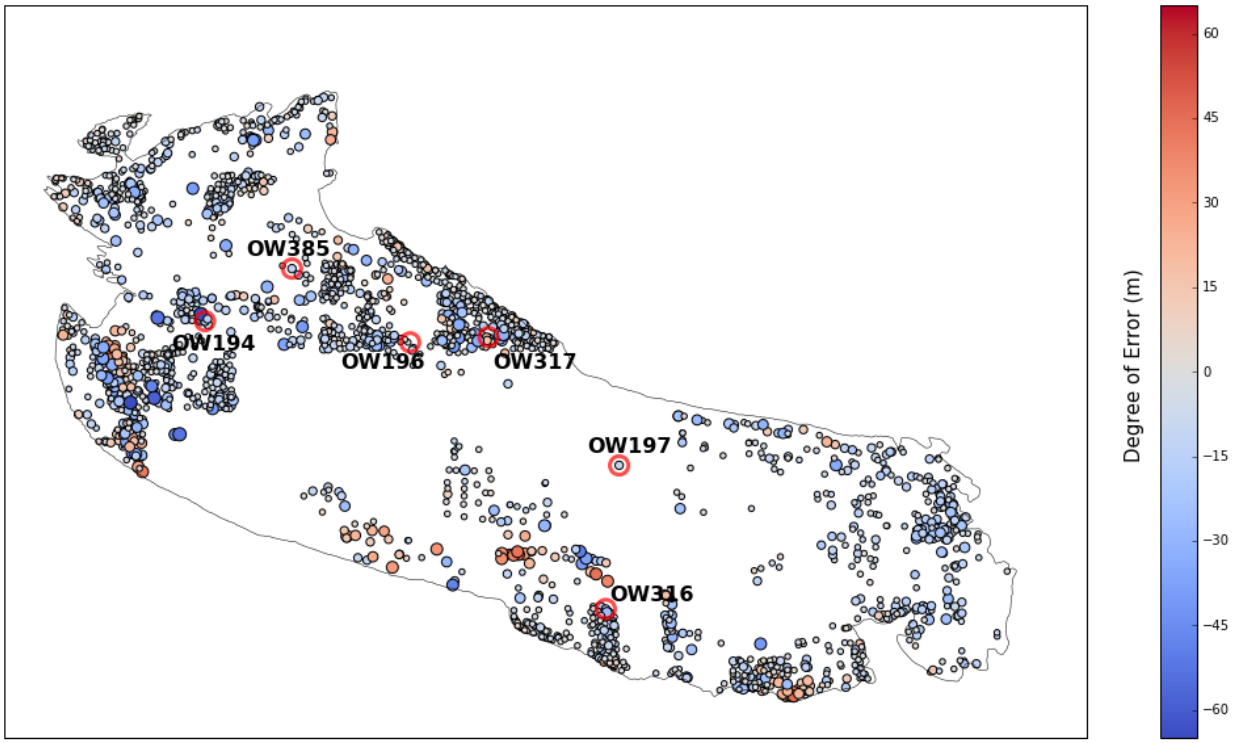

Figure 21. Spatial distribution of error. The colour of the solid circles indicates the magnitude and direction of the residual error (a red colour indicates an under estimation of groundwater level). The size of the solid circles has been scaled to represent the magnitude of the residual (larger circles indicate a higher degree of error). The red hollow circles represent the locations of the observation wells used for the transient calibration.

Overall, model generally over-predicts groundwater levels. Numerous model calibration runs were undertaken in order to try and lower the heads in the observation wells. Efforts included varying the hydraulic conductivity and specific storage of the bedrock, altering the width of the seepage cells at the perimeter of the model domain. The cause for this lack of accuracy is likely due to local heterogeneities in the hydraulic properties in the fractured bedrock, which are not represented in the model due to its regional scale. Hydraulic conductivity can vary significantly at a local scale due to the presence of discrete fractures. The response of a well to stressors, such as seasonal changes in recharge, changes in tide, and pumping, are highly influenced by the occurrence of fractures, even though at a regional scale such features tend to impart so called equivalent hydraulic properties to the aquifer. Similar challenges with model calibration were met by Foster (2014), Larocque (2014) and Trapp (2011). Another possible cause of the elevated groundwater levels is that the model was set to a daily time-step. Heavy precipitation events occurring at a sub-daily time scale are accumulated over a day, decreasing the precipitation intensity simulated by the model. High intensity precipitation can exceed the infiltration capacity of soils, resulting in the occurrence overland flow and reduced recharge. Thus, reducing groundwater levels.

Model Validation

The validation period is used to display the ability of the calibrated model to reproduce real world observations to an acceptable degree. As previously mentioned, the validation period followed the calibration period from October 1st 2005 to September 30th 2015, a ten-year period. Similar to the calibration period, the transient groundwater levels for the validation period were compared to the observation wells and error statistics calculated. The validation results are consistent with the calibration results in that the model generally over-predicts the groundwater levels (see Burgess, in prep for more detailed results).

Sensitivity Analysis

A sensitivity analysis was conducted to assess the individual parameter sensitivity. This helps assess the uniqueness of the model. The sensitivity analysis was carried out by varying, both increasing and decreasing, one selected parameter and holding constant all others. The sensitivity of the selected parameter was qualitatively determined by comparison of the

error statistics between the calibrated model result and the varied parameter result. Due to the length of model runs (>5 hrs) and number of parameters investigated, only one value either side of the calibrated parameter value (e.g. one increased and one decreased parameter value) was used.

Five parameters were varied: LAI, Manning's M, soil UZ thickness, SZ lower level (depth) and the bedrock hydraulic conductivity. Burgess (in prep) discusses the results of the sensitivity analysis in more detail. However, the results indicate that that the hydraulic conductivity and the thickness of the seepage zone have the largest control on the regional groundwater flow system; land surface and unsaturated hydrologic processes are not influential at the regional scale.

4.0 Results

4.1 Water Balance

The water balance of the model simulation was extracted using the water balance tool in MIKE SHE. This tool extracts the average incremental water height equivalent (in mm) of components of the water balance (e.g. evapotranspiration and recharge) for the entire model domain at each time step. This extracted daily water balance dataset was then grouped into water years (WY) instead of calendar years. A water year is used to ensure that precipitation from wet seasons is grouped together, and not split between two different calendar years. A water year runs from October 1st (e.g. 1995-10-01) to September 30th of the next year (e.g. 1996-09-30). The daily water balance was summed for each water year. The summed water balance components of interest (precipitation, actual evapotranspiration, runoff, recharge, and the water balance error) of each water year in the post spin-up period of the calibration phase of the simulation are tabulated in Table 12.

Table 12. Annual (WY) water balance. All values are in mm.

	Precip	AET	Runoff	Recharge	Error
WY 95-96	1000	435	332	189	-22
WY 96-97	1253	431	476	209	-23
WY 97-98	790	381	335	203	-41
WY 98-99	1166	399	471	209	-36
WY 99-00	965	379	356	200	-24
WY 00-01	801	403	235	188	-6
WY 01-02	883	368	326	194	-33
WY 02-03	876	359	305	192	-25
WY 03-04	964	397	281	193	0
WY 04-05	1145	431	451	215	-38
WY Avg.	984	398	357	199	-25
WB %	100	40	36	20	-2.5

The average water year water balance matches relatively well with the water balance estimates in the conceptual model (Section 2.9, Table 5). For ease of comparison, the estimated range and the initial estimate of the water balance components are repeated in Table 13. All of the simulated water balance components are within the estimated ranges and are within five percentage points of the initial estimates. For the simulation, AET had the widest range (35-55% of mean annual precipitation), while recharge displayed the least amount of variability (17-26% of mean annual precipitation). The mean annual simulated recharge to Gabriola Island is 20% of precipitation (or 199 mm/year).

Table 13. Water balance comparison.

Water Balance Component	Estimated Range (% of mean annual precip.)	Initial Estimate (% of mean annual precip.)	Range of Simulation (% of mean annual precip.)	Average of Simulation (% of mean annual precip.)
Evapotranspiration	32 to 60	45	35 to 55	40
Runoff	26 to 50	40	29 to 42	36
Recharge	1 to 62.7	15	17 to 26	20

The average error within the simulation is relatively small (-2.5% of mean annual precipitation). The negative error represents an overall retention of water in the model system. In other words, on average, slightly more water is entering the model than leaving

it. This indicates that one, or any combination of, the following may be resulting in a slight accumulation of water in the model over the simulation period.

1. bedrock hydraulic conductivity is too low – groundwater is not able to move quickly enough through the model.

2. SZ discharge outlet is too thin – groundwater is not exiting the model fully.

Overall, however, the good agreement between the estimated and simulated water balance, and the relatively low error, indicate that the model is sufficiently calibrated.

4.2 Capture Zones

The simulated 50-year well capture zones of all the groundwater wells sampled for tritium are relatively small (Figure 22). The simulated capture zones range in extent between approximately 120 and 330 m for the wells CC3 and CC4, respectively.

The relatively small, simulated capture zones suggest that the majority of the groundwater at the sample points is sourced a short distance from the wells. This suggests that the groundwater is highly mixed, with very little old, tritium depleted groundwater contributing to the groundwater mixture. This conclusion is in agreement with the analysis of the groundwater tritium concentration (see Burgess, in prep), i.e., all the groundwater samples had a measurable concentration of tritium. This demonstrates that the conceptual model the numerical model is based upon is a reasonable representation of the real world system.

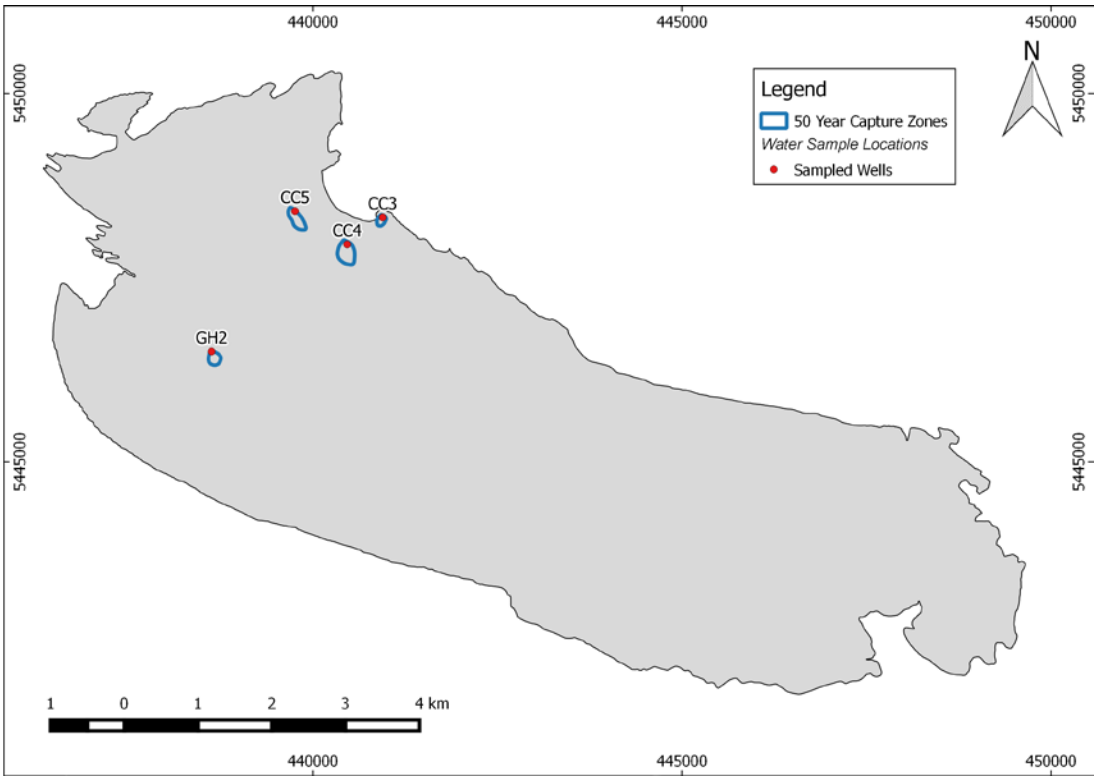

Figure 22. Simulated 50-year well capture zones.

4.3 Spatial and Temporal Variations in Recharge and Seepage

Recharge and seepage vary spatially across the island. Figure 23 shows areas of recharge and discharge on Gabriola Island. Positive values (in blue and green) represent areas where recharge occurs on an average annual basis, while negative values (in red) represent discharge areas. Recharge generally occurs in areas of higher elevation, while seepage occurs in areas of lower, and steeper, topography.

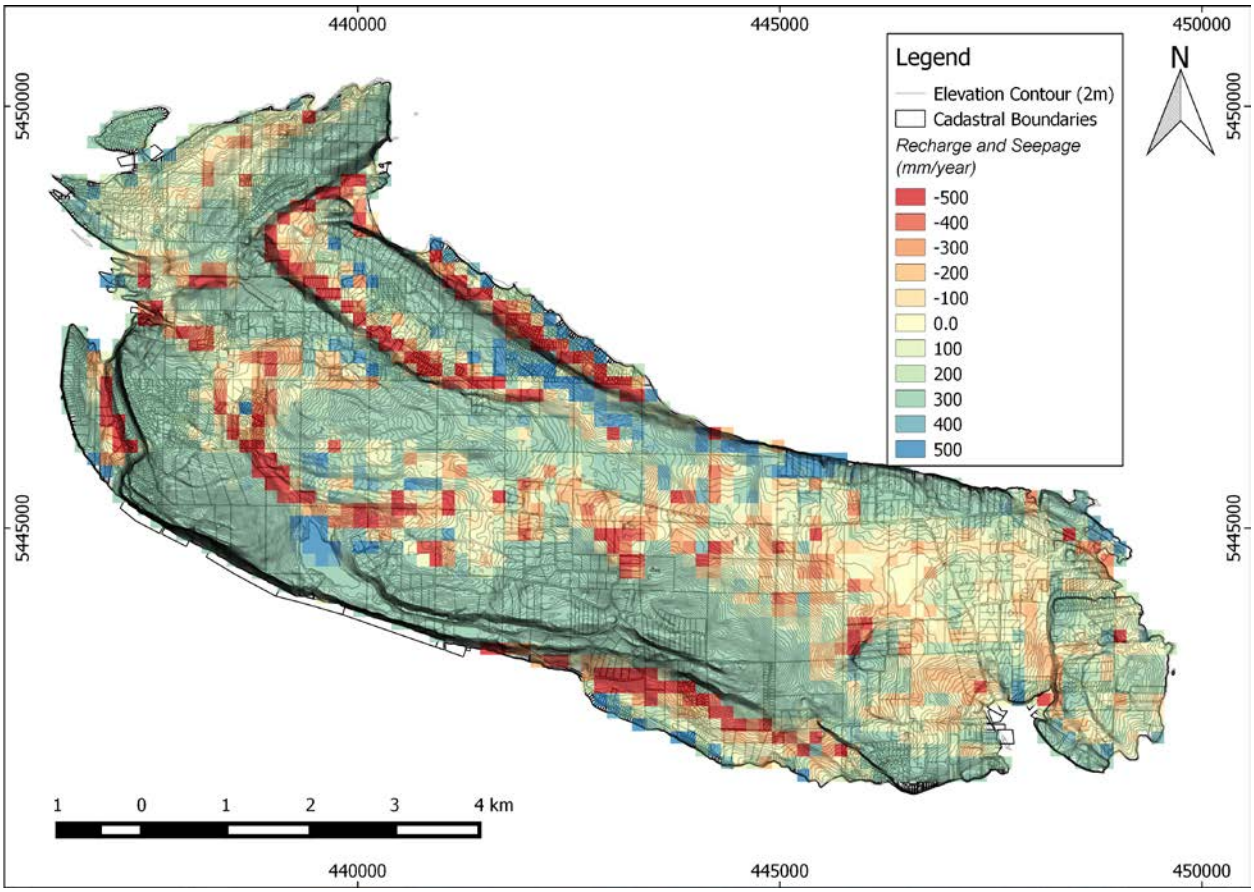

Figure 23. Average annual recharge and seepage (mm/year). The scale shows positive and negative numbers. Positive numbers represent recharge areas on an average annual basis, while negative numbers represent discharge zones on an average annual basis. Values close to zero are neither recharge or discharge areas.

The recharge and discharge patterns vary slightly on a seasonal basis as shown in Figures 24-27 (Fall (SON), Winter (DJF), Spring (MAM) and Summer (JJA), respectively). The overall pattern is consistent with the mean annual recharge and seepage map shown in Figure 23, which suggests that recharge and seepage areas are generally seasonally persistent. The overall magnitude of recharge is much less during the summer as indicated by the near zero values over a larger portion of the island. Seepage during the summer is also somewhat lower.

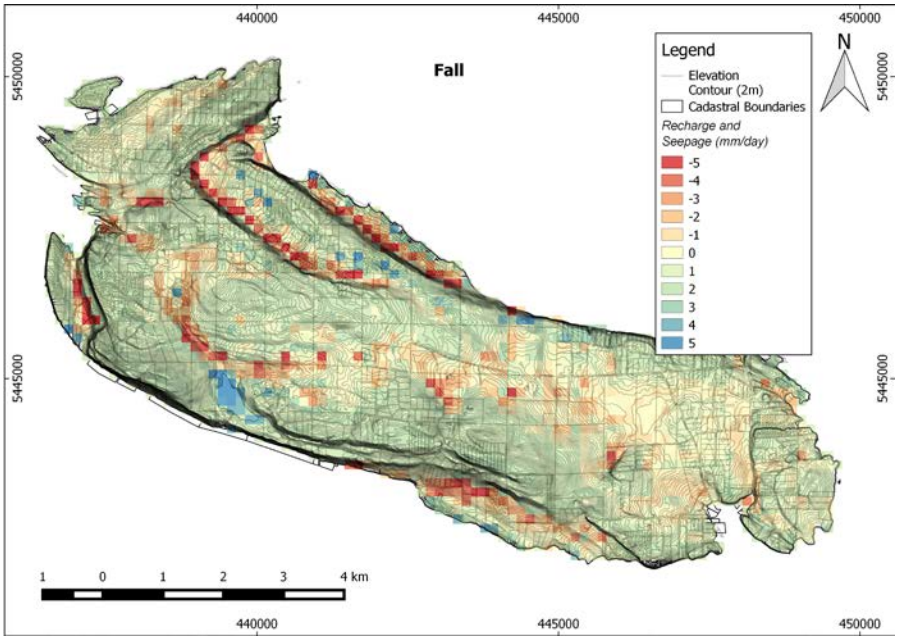

Figure 24. Average Fall recharge and discharge (mm/day). The scale shows positive and negative numbers. Positive numbers represent recharge areas during the fall, while negative numbers represent discharge zones during the fall. Values close to zero are neither recharge or discharge areas.

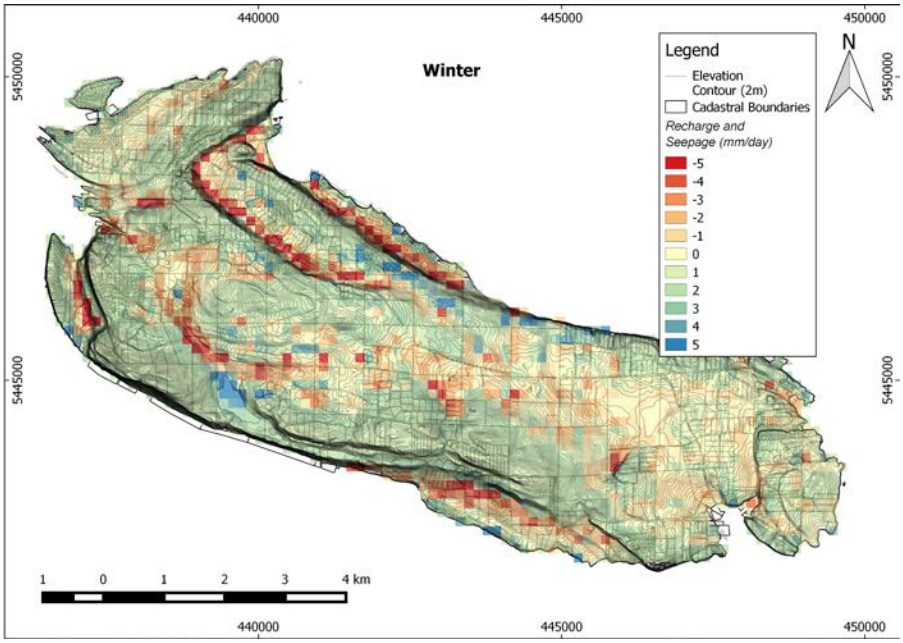

Figure 25. Average Winter recharge and discharge (mm/day). The scale shows positive and negative numbers. Positive numbers represent recharge areas during the winter, while negative numbers represent discharge zones during the winter. Values close to zero are neither recharge or discharge areas.

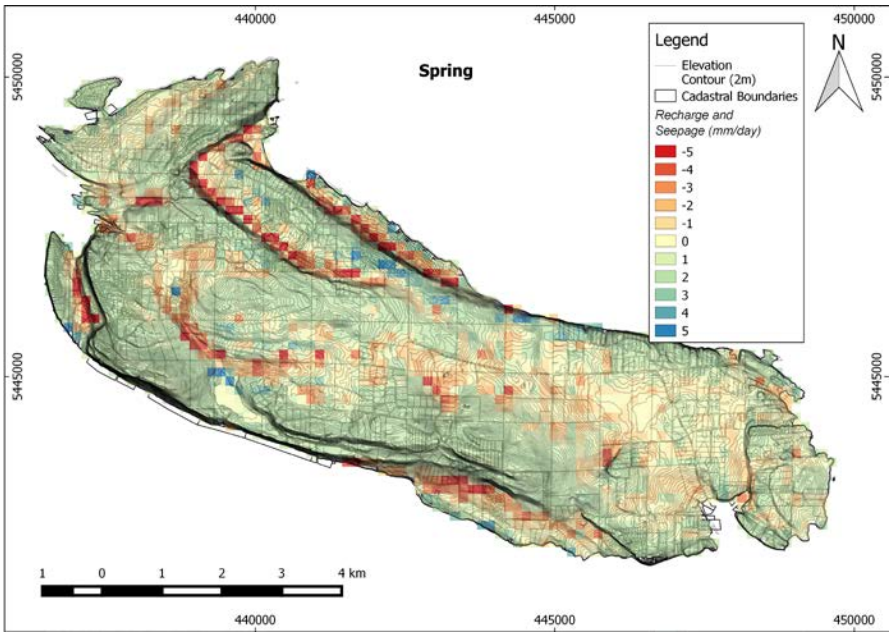

Figure 26. Average Spring recharge and discharge (mm/day). The scale shows positive and negative numbers. Positive numbers represent recharge areas during the spring, while negative numbers represent discharge zones during the spring. Values close to zero are neither recharge or discharge areas.

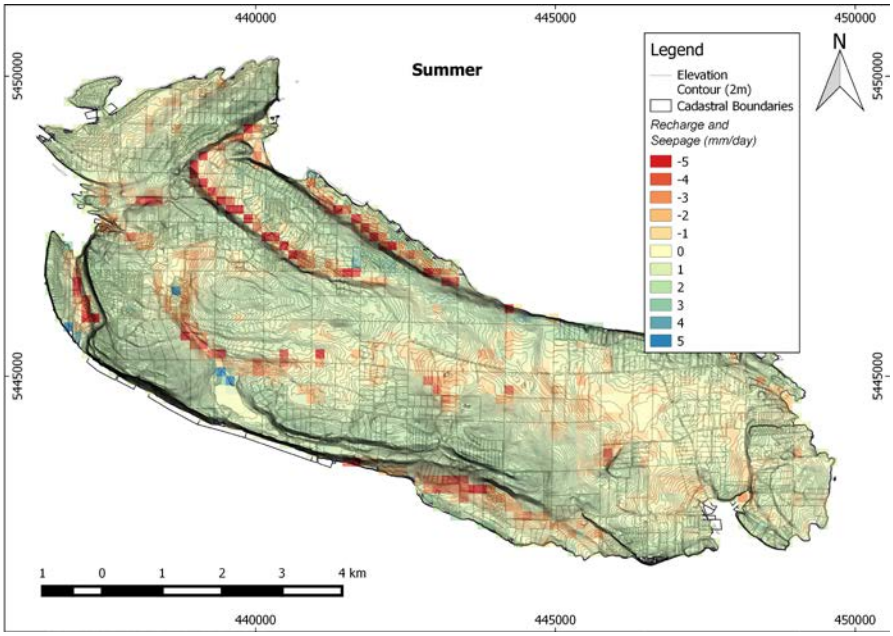

Figure 27. Average Summer recharge and discharge (mm/day). The scale shows positive and negative numbers. Positive numbers represent recharge areas during the summer, while negative numbers represent discharge zones during the summer. Values close to zero are neither recharge or discharge areas.

The seasonal water balance is presented in Figure 28. The overland flow closely matches precipitation; when precipitation is high in winter, runoff is also high. The start of the

increase in overland flow (September) coincides with the increase in precipitation. This increase continues until January, after which both precipitation and overland flow begin to decrease, reaching a low in July and August. Evapotranspiration (ET) is generally low from November to February, and begins to increase in March. ET rises gradually through the summer and begins to drop in August through to October. Recharge increases from October to January, where it reaches a pseudo-stable rate, before declining from April through to September.

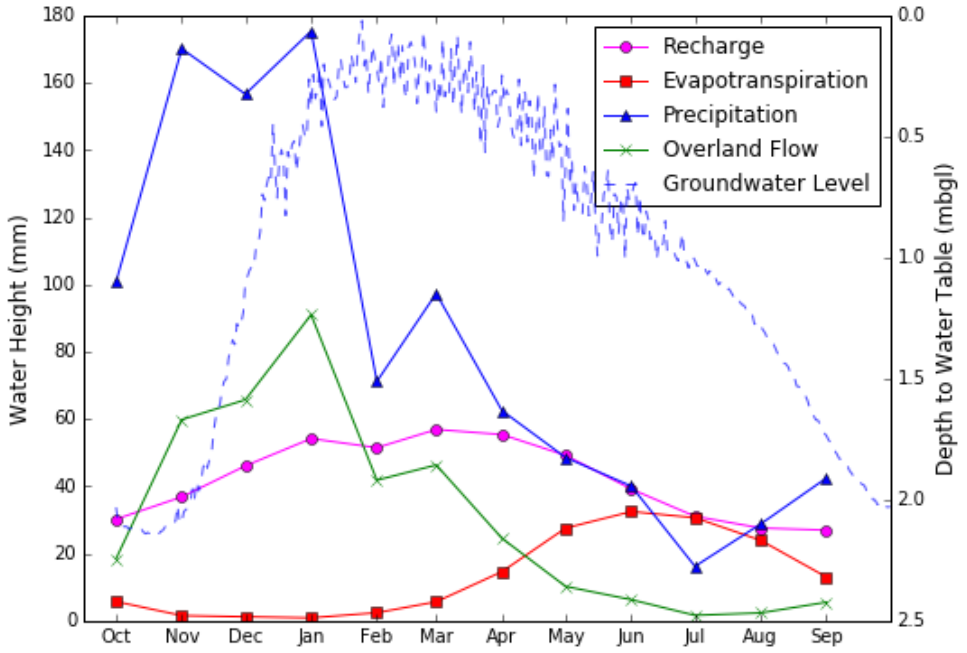

Figure 28. Seasonal simulated water balance. Water balance items are average monthly totals, while the groundwater level is the day of year average for a cell in the model that coincides with the position of observation well 196. Results from the calibration period were used to calculate averages.

The recharge response matches the groundwater level dynamics, with the groundwater level following the same seasonal trend. The groundwater level is shown in Figure 28 as "day of the year average" at a cell in the model that corresponds to the location of Observation Well 196. The groundwater level is represented as the depth to water table (right y-axis). From January to March, the groundwater level is at its highest; just below ground surface. Groundwater levels gradually drop, reaching a low in September. There appears to be a lag time between the increase in precipitation (and overland flow) and the increase in recharge and groundwater level. The increase in precipitation starts in September, while the recharge

rate and groundwater level do not begin to increase until November, representing an approximate 2-month lag time. This lag is caused by the low hydraulic conductivity of the bedrock, which slows the vertical movement of the infiltrating water. Due to the low storage capacity of the bedrock, once the infiltrating water reaches the water table, the pore space quickly fills up and the water table rises rapidly.

4.4 Future Recharge

Under future climate conditions, recharge and other components of the water balance experience variable changes. A comparison between select water balance components under current and future climate conditions is presented in Figure 29.

Each component of the water balance is projected to change under future climate conditions.

- Precipitation is projected to increase in most months, but remain relatively unchanged in the summer. Precipitation amounts are similar for the 2050s and 2080s.
- ET is projected to increase in all months except November to January when RET is projected to change little (Table 8). The projections are similar for the 2050s and the 2080s.
- Overland flow (runoff) is projected to be similar to current conditions for all months, except from December to February. In the 2050s, the runoff is projected to be slightly higher in January, but by the 2080s, runoff is projected to be higher from November to January.
- Recharge is projected to increase slightly from January to March (<5 mm more recharge) with the slightly more recharge occurring in the 2080s compared to the 2050s, but decrease in most other months, particularly in the summer (~10 mm less recharge). Since precipitation is not significantly different in summer, the lower recharge at this time of year is attributed to the significant increase in ET. Overall, the total average annual recharge is projected to decrease under future climate conditions, by approximately 8% and 7% for the 2050s and 2080s, respectively.

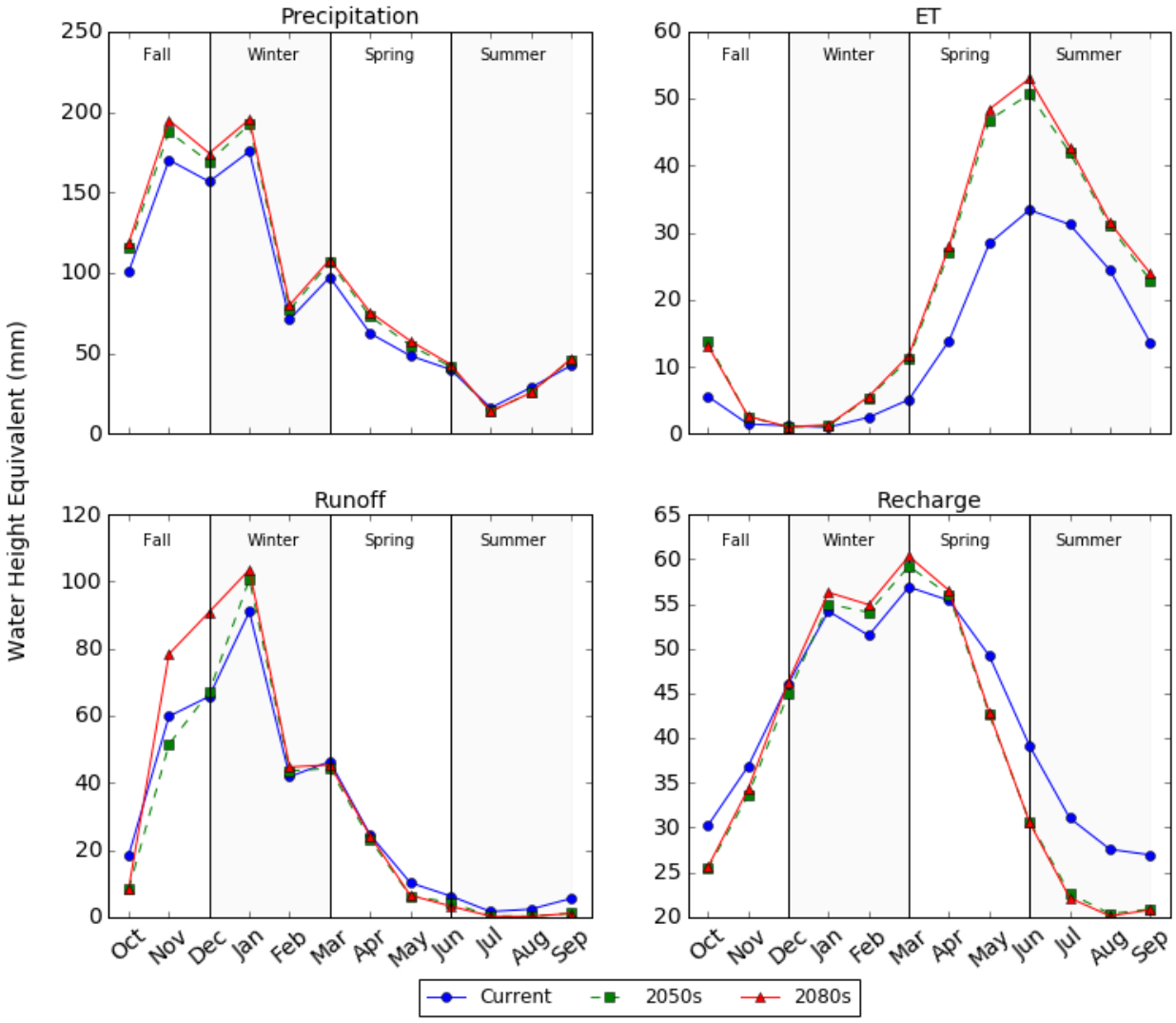

Figure 29. Model water balance under current and future climate conditions. Water balance components are average monthly totals. The calibration period was used as the dataset for averaging.

4.5 Model Limitations

An integrated numerical GW-SW model is ideally suited to understanding and estimating recharge at a regional scale. However, there are important limitations these regional scale models:

- The availability and uncertainty in input parameters. Integrated GW-SW models are highly parameterized and require data that may not available everywhere, or at all, in the model domain (e.g. van Genuchten parameters of fractured bedrock are not available from field and laboratory studies and

these were estimated from previous modeling studies). Thus, assumptions regarding many parameters had to be made.

- Some processes occurring at a smaller scale, such as localised rapid recharge in areas of intensely fractured bedrock, are not represented in the model. The degree to which local processes influence groundwater levels is unknown.

Nevertheless, numerical models are invaluable as they have the ability to investigate the broader scale processes, such as controls on recharge dynamics, and how sensitive the hydrologic system is to future climate variability. These two topics are explored in more detail in the following chapter.

5.0 Conclusions

An integrated surface water-groundwater numerical model was developed using MIKE SHE to investigate recharge on Gabriola Island, under current and future climate conditions.

The model was calibrated to groundwater levels only. The calibrated model over predicted the groundwater levels, but was able to replicate the seasonal dynamics important to this study. The over prediction may be caused by local heterogeneities in bedrock fractures that were unable to be represented at the regional scale of the model.

Recharge and seepage vary spatially across the model domain. Recharge generally occurs in areas of higher elevation, while seepage occurs in areas of both lower and steeper topography. The model developed did not include spatially varying vegetation cover, geology, or soil cover. However, sensitivity analysis results suggest that recharge is most sensitive to the hydraulic conductivity of the fractured bedrock, followed by thickness of the seepage face. Changes in soil cover and vegetation cover did not have a significant impact on recharge.

The model results indicate the recharge and seepage vary temporally throughout an average year. Recharge increases from October to January, where it reaches a pseudo-stable rate,

before declining from April through to September. Recharge appears to lag the seasonal precipitation by approximately 2 months.

Under future climate conditions, mean annual recharge is projected to decrease by approximately 8% and 7% in the 2050s and 2080s, respectively. However, most of this decrease will occur during the already dry summer months (5 to 10 mm/month). This reduction in recharge in the summer is caused by a significant increase in evapotranspiration at this time of year. In winter, monthly recharge is projected to increase due to increased precipitation, but only by less than 5 mm/month. Most of the increase in precipitation will result in increased overland flow.

6.0 Acknowledgements

This research was supported by a grant to Simon Fraser University by the Regional District of Nanaimo and the Gabriola Island Local Trust Committee of the Islands Trust. Additional funding was provided by Simon Fraser University and a Natural Sciences and Engineering Research Council Discovery Grant to Dr. Allen.

7.0 References

Allen, D.M. and Kirste, D. 2012. Results of the July 2011 Groundwater Chemistry Sampling Study on Mayne Island, British Columbia. Report prepared for the Mayne Island Integrated Water Systems Society. Simon Fraser University, Burnaby, BC, 39 pp.

Allen, D.M. and Liteanu, E. 2008. Long-term Dynamics of the Saltwater-Freshwater Interface on the Gulf Islands, British Columbia, Canada. In. G. Barrocu (Ed.) Proceedings of the First International Joint Saltwater Intrusion Conference, SWIM-SWICA, Cagliari, Italy, September 25-29, 2006.

Allen, D.M., Liteanu, E., Bishop, T.W., and Mackie, D.C., 2002. Determining the hydraulic properties of fractured bedrock aquifers of the Gulf Islands, B.C. Final report. Department of Earth Sciences, Simon Fraser University. Submitted to BC Ministry Water, Land and Air Protection.

Allen, D.M. and Matsuo, G.P., 2001. Results of the Groundwater Geochemistry Study on Hornby Island, British Columbia. Report prepared for the Islands Trust, Victoria, B.C., 119 pp.

Allen, D.M. and Suchy, M. 2001. Results of the groundwater geochemistry study on Saturna Island, British Columbia. Report submitted to the Island Trust, Victoria, B.C., 127 pp.

Anderson, P., Woessner, W. W., Hunt, R. 2015. *Applied Groundwater Modeling: Simulation of Flow and Advective Transport.* San Diego, CA: Academic Press.

Appaih-Adjei, E.K. 2006. *Climate change impacts on groundwater recharge in Gulf Islands, Canada* (Master dissertation). Lund University, Lund, Sweden.

Black, T.A. 1979. Evapotranspiration from Douglas Fir stands exposed to soil water deficits. *Water Resources Research*, 15(1).

BC Ministry of Energy and Mines. 2005a. Geofile 2005-3, by N.W.D. Massey, D.G. MacIntyre, P.J. Desjardins and R.T. Cooney.

BC Ministry of Environment (MoE). 2015b. WELLS Database. Water Stewardship Division, BC. Retrieved from http://www.env.gov.bc.ca/wsd/data_searches/wells/ [Accessed August, 2015].

BC Ministry of Environment (MoE). 2015. Province of British Columbia, British Columbia Soil Mapping Spatial Data (a compilation of digital soil mapping datasets). Data available from the British Columbia Ministry of Environment, Ecosystem Information Section at: http://www.env.gov.bc.ca/esd/distdata/ecosystems/Soil_Data/SOIL_DATA_FGDB/ [Accessed September 14th, 2015]

BC Ministry of Forests, Lands and Natural Resource Operations (FLNRO). 2011. Baseline Thematic Mapping Present Land Use Version 1 Spatial Layer. Published by Ministry of Forests, Lands and Natural Resource Operations (FLNRO).

Burgess, R. (in prep). Characterizing Recharge to Fractured Bedrock in a Temperate Climate. Department of Earth Sciences, Simon Fraser University.

Cannon, A. J. 2008. Probabilistic multi-site precipitation downscaling by an expanded Bernoulli-gamma density network, *J. Hydrometerol*, 9(6), 1284–1300.

Carlsson H., Carlsson L., Jamtlid A., Nordlander H., Olsson O., Olsson T., 1983. Cross-hole techniques in a deep seated rock mass. *Bulletin of the Int. Assoc. Eng. Geol.* 26, pp. 377–384.

Carter, T.R., E.L. La Rovere, R.N. Jones, R. Leemans, L.O. Mearns, N. Nakićenović, A.B. Pittock, S.M. Semenov, and J. Skea. 2001: Developing and applying scenarios. In: *Climate Change 2001: Impacts, Adaptation, and Vulnerability. Contribution of Working Group II to the Third Assessment Report of the Intergovernmental Panel on Climate Change* [McCarthy, J.J., O.F. Canziani, N.A. Leary, D.J. Dokken, and K.S. White (eds)]. Cambridge University Press, Cambridge and New York, pp. 145-190

Chiew, F. H. S., and McMahon, T. A. 1991. The applicability of Morton's and Penman's evapotranspiration estimates in rainfall-runoff modeling. *Water Resources Bulletin, AWRA, August 2001.* 27, No. 4.

Clague, J.J. 1983. Glacio-isostatic effects of the Cordilleran ice sheet, British Columbia. In: *Shorelines and Isostacy*, eds. D.E Smith and A.G. Dawson. London: Academic Press.

Cranfield University Silsoe. 2002 . AWSET (Version 3.0)

Dakin, R.A., Farvolden, R.N., Cherry, J.A., and Fritz, P. 1983, Origin of dissolved solids in groundwaters of Mayne Island, British Columbia, Canada: *Journal of Hydrology*, v. 63, p. 233–270.

Denny, S., Allen, D.M. and Journeay, M. 2007. DRASTIC-Fm: A modified vulnerability mapping method for structurally controlled aquifers in the southern Gulf Islands, British Columbia, Canada. *Hydrogeology Journal, 15*, 483-493.

DHI. 2007. MIKE SHE User Manual, Volume 2: Reference Guide, Danish Hydraulic Institute: Denmark.

Earle S. and E. Krogh. 2004. Geochemistry of Gabriola's groundwater, Shale: Journal of the Gabriola, Historical & Museum Society, No. 7, Jan 2004

EBA. 2011. Geohazard Report and Mapping, Gabriola Island, BC. Report to Islands Trust.

England T.D.J. 1989. Late Cretaceous to Paleogene evolution of the Georgia Basin, southwestern British Columbia, Ph.D. thesis, Memorial University of Newfoundland.

Environment Canada. 2015. Historical climate data and climate normals. http://climate.weather.gc.ca/ (accessed January 2015).

Fernandes, R., Korolevych, V., and Wang, S. 2007. Trends in land evapotranspiration over Canada for the period 1960–2000 based on in situ climate observations and a land surface model. *J. of Hydrometeorology*. 18.

Foster S., 2014. *Characterizing groundwater – surface water interactions within a mountain to ocean watershed, Lake Cowichan, British Columbia.* M.Sc. Thesis. (MSc Thesis). Simon Fraser University, BC, Canada.

Gleeson, T., Smith, L., Moosdorf, N., Hartmann, J., Dürr, H.H., Manning, A.H., van Beek, L.P.H., Jellinek, A.M. 2011. Mapping permeability over the surface of the Earth. Geophys. Res. Lett. 38

Green, T. M. Taniguchi, H. Kooi, J. Gurdak, K. Hiscock, D. Allen, H. Treidel, A. Aureli. 2011. Beneath the surface of global change: Impacts of climate change on groundwater. *Journal of Hydrology*, 405: 532-560.

Hodge, W.S. 1977. A preliminary geohydrological study of Saltspring Island. Groundwater Section, Hydrology Division, Water Investigations Branch, BC Ministry of Environment.

Hodge W.S. 1978. A Review of Groundwater Conditions on Gabriola Island. BC Ministry of the Environment, Water Investigations Branch, Victoria BC.

Hodge, W.S. 1995. Groundwater conditions on Saltspring Island. Groundwater Section, Hydrology Branch, Water Management Division, Ministry of Environment, Land and Parks

Jaber, F. H., and Shukla, S. 2012. MIKE SHE: Model use, calibration, and validation. *Transactions of the ASABE*, 55(4), 1479-1489.

Journeay, J.M. and Morrison, J. 1999. Field investigation of Cenozoic structures in the northern Cascadia forearc, southwestern British Columbia. In *Current Research* 1999-A, Geological Survey of Canada, Ottawa, ON, pp.239-250.

Jiang, X.W., Wang, X.S., and Wan, L. 2010. Semi-empirical equations for the systematic decrease in permeability with depth in porous and fractured media. *Hydrogeology Journal.* 18(4): p. 839-850.

Kenney, A.E. and van Vliet, L.J.P. 1986. Gabriola Island (Interim) Soil Inventory. BC Ministry of Environment, Land Resource Unit.

Larocque, I. 2014. *Hydrogeology of Salt Spring Island, British Columbia* (MSc thesis). Simon Fraser University, Canada.

Leij, F. J. 1996. The UNSODA unsaturated soil hydraulic database: User's manual. Cincinnati, Ohio: National Risk Management Research Laboratory, Office of Research and Development, U.S. Environmental Protection Agency. Retrieved from http://hdl.handle.net/2027/mdp.39015050283400

Liteanu, E. 2003. *The role of aquifer heterogeneity in saltwater intrusion modeling, Saturna Island, BC, Canada* (MSc thesis). Simon Fraser University, Vancouver, Canada.

Liu, J., Chen, J. M., Cihlar, J. 2003. Mapping evapotranspiration based on remote sensing: An application to Canada's landmass. *Water Resources Research.* Vol. 39, No. 7.

Mackie, D.C. 2002. *An integrated structural and hydrogeologic investigation of the fracture system in the upper Cretaceous Nanaimo Group, southern Gulf Islands, British Columbia* (MSc thesis). Simon Fraser University, Vancouver, Canada.

Meidinger, D. V., and Pojar, J. 1991. Ecosystems of British Columbia. Special report series, B.C. Ministry of Forests.

Monteith, J. L. 1981. Evaporation and temperature. *Q. J. Royal Meteo. Soc*. 107:1-27.

Mustard, P.S. 1994. The upper Cretaceous Nanaimo Group, Georgia Basin. *Geology and Geological Hazards of the Vancouver Region, southwestern British Columbia*, bulletin 481, 27-95.

Nuszdorfer, F.C., Klinka, K., Demarachi, D.A. 1991. Ecosystems of British Columbia. Special report series, Chapter 5, B.C. Ministry of Forests.

Oda, M. 1986. An equivalent continuum model for coupled stress and fluid flow analysis in jointed rock masses. *Water Res* 22, pp. 1845–1856.

Pacific Climate Impacts Consortium (PCIC). 2016. Regional analysis tool. Retrieved from http://www.pacificclimate.org/analysis-tools/regional-analysis-tool, January, 2016.

Penman, H. L. 1948. Natural evaporation from open water, bare soil and grass. Proceedings of the Royal Society of London. *Series A, Mathematical and Physical Sciences*, 193(1032), 120-145.

Rathay S. in prep. *Response of a fractured bedrock aquifer to recharge from heavy rainfall events.* M.Sc. Thesis. (MSc Thesis). Simon Fraser University, BC, Canada.

Snow, D. T. 1968. Rock fracture spacings, openings, and porosities. *J Soil Mech found Div ASCE. 96.*

Spittlehouse, D. L. and Black, T. A. 1979. Determination of forest evapotranspiration using Bowen ratio and eddy correlation measurements, *J of Applied Meteorology and Climatology*. 18.

SRK Consulting. 2013. Water Budget Project: RDN Phase One (Gabriola, DeCourcy & Midge Islands). Report to Regional District of Nanaimo, April 2013.

Stober, I. 2011, Depth and pressure-dependent permeability in the upper continental crust: Data from the Urach 3 geothermal borehole, southwest Germany. *Hydrogeology Journal*. 19(3): p. 685-699.

Surrette, M., Allen, D.M. and Journeay, M. 2008. Regional evaluation of hydraulic properties in variably fractured rock using a hydrostructural domain approach. Hydrogeology Journal, 16(1): 11-30. doi:10.1007/s10040-007-0206-9

Thomas, S.C. and Winner, W.E. 2000. Leaf area index of an old-growth Douglas-fir forest estimated from direct structural measurements in the canopy. *Can. J. For. Res.* 30: 1922–1930.

Trapp, A. 2011. *Constraining a density-dependent groundwater flow model using multiple calibration time periods* (Masters dissertation). Universität Stuttgart, Stuttgart, Germany. (thesis work completed at SFU).

Trofymow, J. A., Porter, G. L., Blackwell, B. A., Arksey, R., Marshall, V., and Pollard, D. 1997. Chronosequences for research into the effects of converting coastal British Columbia old-growth forests to managed forests: an establishment report (Inf. Rep. BC-X-374). Victoria, B.C., Canada: Natural Resources Canada, Canadian Forest Service, Pacific Forest Centre

United States Department of Agriculture (USDA). 1986. Urban hydrology for small watersheds. Technical release 55 (TR-55). June, 1986. Table 3-1.

Voeckler, H.M., Allen, D.M. and Alila, Y. 2014. Modeling coupled surface water – groundwater processes in a small mountainous headwater catchment. *Journal of Hydrology, 517.*

Wei, Z. Q., Egger, P., Descoeudres, F. 1995. Permeability predictions for jointed rock masses. *Int J Rock Mech Min Sci Geomech* 3, pp. 251–261.

Welch, L.A. and Allen, D.M. 2012. Consistency of groundwater flow patterns in mountainous topography: Implications for valley-bottom water replenishment and for defining hydrogeological boundaries. *Water Resources Research,* 48.

Welyk T.J. and Baldwyn J. 1994. Gabriola, Valdez, Thetis and Kuper Islands, Well Allocation Plan, March 1994, Regional Water Management, Vancouver Island Region, Nanaimo BC.

Zhang, L., Hickel, K., Dawes, W.R., Chiew, F. H. F., Wester, A. W., and Briggs, P. R. 2004. A rational function approach for estimating mean annual evapotranspiration. *Water Resources Research.* Vol 40, Issue 2.